AIP | Review of Scientific Instruments

Ultrafast optical parametric amplifiers

Giulio Cerullo and Sandro De Silvestri

Citation: Review of Scientific Instruments **74**, 1 (2003); doi: 10.1063/1.1523642
View online: http://dx.doi.org/10.1063/1.1523642
View Table of Contents: http://scitation.aip.org/content/aip/journal/rsi/74/1?ver=pdfcov
Published by the AIP Publishing

REVIEW ARTICLE

Ultrafast optical parametric amplifiers

Giulio Cerullo and Sandro De Silvestri[a)]
Istituto Nazionale per la Fisica della Materia, IFN-CNR, Dipartimento di Fisica, Politecnico, I-20133 Milano, Italy

(Received 26 October 2001; accepted 27 July 2002)

Over the last decade there have been spectacular developments in ultrafast laser technology, due to the introduction of solid state active materials and of new mode-locking and amplification techniques. These advances, together with the discovery of new nonlinear optical crystals, have fostered the introduction of ultrafast optical parametric amplifiers as a practical source of femtosecond pulses tunable across the visible and infrared spectral ranges. This article summarizes the recent progress in the development of ultrafast optical parametric amplifiers, giving the basic design principles for different frequency ranges and in addition presenting some advanced designs for the generation of ultrabroadband, few-optical-cycle pulses. Finally, we also briefly discuss the possibility of applying parametric amplification schemes to large-scale, petawatt-level systems. [DOI: 10.1063/1.1523642]

I. INTRODUCTION

Ultrafast optical science is a rapidly evolving multidisciplinary field: the ability to excite matter with femtosecond light pulses and probe its subsequent evolution on ultrashort time scales opens up completely new fields of research in physics, chemistry, and biology.[1] Furthermore, the high intensities that can be generated using femtosecond light pulses allow us to explore new regimes of light-matter interaction.[2] The implementation of more sophisticated spectroscopic techniques has been accompanied by improvements in laser sources. Considerable effort has been dedicated to the achievement of shorter light pulses,[3–5] to improve temporal resolution; other efforts have worked to expand the frequency tunability of the pulses, since this would make it possible to excite in resonance different materials, and to probe optical transitions occurring at different frequencies. Early sources of femtosecond optical pulses were based on dye laser technology;[6] in that case, some frequency tunability could be achieved by simply changing the laser dye. This flexibility, however, came at the expense of a complicated and time consuming reoptimization.

The 1990s have witnessed a revolution in ultrafast laser technology, thanks to the advent of solid state active materials, such as Ti:sapphire, and powerful mode-locking techniques, such as Kerr lens mode locking (KLM).[7] With these advances, femtosecond lasers have gained tremendously in reliability and user-friendliness, becoming ''turnkey'' devices available to a wide community of nonspecialists. Another landmark of femtosecond technology has been the chirped pulse amplification (CPA) technique,[8,9] which enabled increasing the energy of femtosecond lasers by 2–3 orders of magnitude, from the millijoule to the multijoule level. This increase in peak power makes it possible to access a whole new class of nonlinear optical phenomena, triggering a renaissance in the field of nonlinear optics. Parallel to these developments has been the discovery of novel nonlinear optical crystals, such as β-barium borate (BBO) and lithium triborate (LBO),[10–14] combining improved optical characteristics (high nonlinear optical coefficients, low group velocity dispersion, broad transparency ranges) with high damage thresholds.

KLM Ti:sapphire lasers amplified by the CPA technique are now widely used sources of stable, energetic femtosecond pulses: however, their frequency tunability is limited to a narrow range around the fundamental wavelength (FW) of 0.8 μm or around the second harmonic (SH) of 0.4 μm. Their tuning range can be greatly extended by using optical parametric generation (OPG).[15–19] The principle of OPG is quite simple: in a suitable nonlinear crystal, a high frequency and high intensity beam (the *pump* beam, at frequency ω_p) amplifies a lower frequency, lower intensity beam (the *signal* beam, at frequency ω_s); in addition a third beam (the *idler* beam, at frequency ω_i, with $\omega_i < \omega_s < \omega_p$) is generated.[20] In the interaction, energy conservation

$$\hbar\omega_p = \hbar\omega_s + \hbar\omega_i \tag{1}$$

is satisfied; for the interaction to be efficient, also the momentum conservation (or phase matching) condition

$$\hbar\mathbf{k}_p = \hbar\mathbf{k}_s + \hbar\mathbf{k}_i, \tag{2}$$

where $\mathbf{k}_p$, $\mathbf{k}_s$, and $\mathbf{k}_i$ are the wave vectors of pump, signal, and idler, respectively, must be fulfilled. The signal frequency to be amplified can vary in principle from $\omega_p/2$ (the so-called degeneracy condition) to ω_p, and correspondingly the idler varies from $\omega_p/2$ to 0; at degeneracy, signal and

a)Electronic mail: sandro.desilvestri@polimi.it

idler have the same frequency. In summary, the OPG process transfers energy from a high-power, fixed frequency pump beam to a low-power, variable frequency signal beam, thereby generating also a third idler beam. To be efficient, this process requires very high intensities of the order of tens of GW/cm^2; it is therefore eminently suited to femtosecond laser systems, which can easily achieve such intensities even with modest energies, of the order of a few microjoules.

OPG can be exploited in two ways to achieve frequency tunability: if the OPG crystal is enclosed in a suitable optical cavity and the parametric gain exceeds the losses, the cavity starts oscillating like an ordinary laser and an optical parametric oscillator (OPO) is obtained. A completely different approach consists in amplifying a suitably generated weak signal beam (the so-called ''seed'' beam) in one or more OPG crystals, thus obtaining an optical parametric amplifier (OPA). Both schemes are employed with ultrashort pulses, as well as in continuous wave (cw) and nanosecond pulse systems, and each has its advantages and drawbacks. OPOs can be pumped by a small-scale femtosecond oscillator, and provide pulses at very high repetition rates ($\approx$100 MHz). This helps in experiments detecting very weak signals to improve signal-to-noise ratio.[21–24] On the other hand, OPO output energies are low (typically a few nanojoules), and they require a cavity whose length is matched to that of the pump laser to within micrometers. Their tunability is limited by the bandwidth of the mirror coatings, so that several mirror sets may be required to span the whole tuning range. OPAs require high pump intensities, provided only by an amplified system, and operate at lower repetition rates (typically from 1 to 100 kHz); on the other hand, they provide high output energies, broad frequency tunability and are simpler to operate, since they do not require any cavity length stabilization. Therefore, femtosecond OPOs and OPAs are complementary systems, used in different types of applications.

In this article we will deal exclusively with femtosecond OPAs, which have become the most widespread source of tunable femtosecond pulses and have reached a high level of stability and reliability, becoming true workhorses of ultrafast spectroscopy. These systems are usually pumped by an amplified Ti:sapphire laser, providing pulses with millijoule-level energy, $\approx$100 fs duration and kilohertz repetition rate; pumping can occur either at the FW or at the SH of the laser beam. Femtosecond OPAs have demonstrated tunability from the ultraviolet (UV) to the mid-infrared (IR), and produce pulse energies up to the 100 μJ level. In addition, femtosecond OPAs have the capability of generating pulses significantly shorter than the pump pulses, exploiting the broad gain bandwidths available in the parametric interaction. They can therefore be used as effective pulse compressors. Recently ultrabroadband pulses with duration down to $\approx$5 fs in the visible and $\approx$15 fs in the near-IR have been demonstrated containing only a few optical cycles of the carrier frequency.

This article will review the substantial recent progress in the field of femtosecond OPAs, giving the basic design principles for different frequency ranges, and in addition presenting some advanced designs and perspectives for future developments. The article is organized as follows: in Sec. II we briefly review the theory of optical parametric amplification and point out the main issues related to optical parametric amplification of ultrashort pulses. In Sec. III we present some specific OPA designs, with different tuning ranges (visible, near-infrared, mid-infrared, and ultraviolet). In Sec. IV we describe more advanced, ultrabroadband OPA designs for the generation of few-optical-cycle light pulses in the visible and near-infrared. In Sec. V we introduce the concept of optical parametric chirped pulse amplification (OPCPA), which holds the promise of scaling the power of amplified ultrashort pulse systems to the multipetawatt level. Finally, in Sec. VI conclusions are drawn and prospects for future developments are discussed.

II. THEORY OF OPTICAL PARAMETRIC AMPLIFICATION

A. The optical parametric amplification process

In the following we will briefly derive the coupled nonlinear equations describing the optical parametric amplification process.[15–19] We start with a linearly polarized, monochromatic plane wave at frequency ω, propagating in the z direction

$$E(z,t)=\mathrm{Re}\{A(z)\exp[j(\omega t-kz)]\}, \tag{3}$$

in a medium with nonlinear polarization, at the same frequency,

$$P^{nl}(z,t)=\mathrm{Re}\{P^{nl}(z)\exp[j(\omega t-k_p z)]\}. \tag{4}$$

Within the slowly-varying-amplitude approximation $[(d^2A/dz^2)\ll 2k(dA/dz)]$ we can derive the following propagation equation:

$$\frac{dA}{dz}=-j\frac{\mu_0 c_0 \omega}{2n}P^{nl}\exp[-j(k_p-k)z], \tag{5}$$

where c_0 is the speed of light in vacuum and n is the refractive index at frequency ω. Equation (5) shows that the nonlinear polarization acts as a source term driving the amplitude variations of the propagating wave.

Let us now consider the interaction of three waves, at frequencies ω_p, ω_s, and ω_i, with $\omega_i<\omega_s<\omega_p$ and $\omega_i+\omega_s=\omega_p$, in a medium with second order nonlinear polarization. The component of the nonlinear polarization vector along direction i is expressed as

$$P_i^{nl}=\epsilon_0\chi_{ijk}^{(2)}E_jE_k, \tag{6}$$

where i, j, and k each take the values x, y, and z, $\chi^{(2)}$ is the third-rank (27 components) second-order nonlinear susceptibility tensor and the Einstein summation convention is used. For the moment we will assume that the three beams are collinear, i.e., with parallel wave vectors, although in general their polarization will be different. We will, however, see later that the noncollinear interaction geometry is important and is used to achieve ultrabroad amplification bandwidths. We can now easily derive the following coupled equations[18,19]

$$\frac{dA_i}{dz}=-j\frac{\omega_i d_{\mathrm{eff}}}{n_i c_0}A_s^*A_p\exp(-j\Delta kz), \tag{7a}$$

$$\frac{dA_s}{dz} = -j\frac{\omega_s d_{\text{eff}}}{n_s c_0} A_i^* A_p \exp(-j\Delta k z), \tag{7b}$$

$$\frac{dA_p}{dz} = -j\frac{\omega_p d_{\text{eff}}}{n_p c_0} A_i A_s \exp(j\Delta k z), \tag{7c}$$

where d_{eff} is the so-called effective nonlinear optical coefficient, depending on the propagation direction and the polarization of the three beams, and $\Delta k = k_p - k_s - k_i$ is the so-called wave-vector mismatch. Equations (7) describe a wealth of second-order nonlinear optical phenomena, such as sum frequency generation, second harmonic generation, difference frequency generation, and optical parametric amplification. By some straightforward manipulations, these three coupled equations can be cast into the form

$$\frac{1}{\omega_i}\frac{dI_i}{dz} = \frac{1}{\omega_s}\frac{dI_s}{dz} = -\frac{1}{\omega_p}\frac{dI_p}{dz}, \tag{8}$$

where $I_j = \frac{1}{2}\epsilon_0 C_0 M_j |A_j|^2$ is the intensity of the beam at frequency ω_j. Equations (8), also known as Manley–Rowe relationships, state photon conservation and show that the three-wave interaction in second-order nonlinear media manifests itself in the energy flow from the two lower-frequency fields to the sum-frequency field or vice versa. In the case of sum-frequency generation, two powerful beams at ω_i and ω_s interact to produce a beam at the sum frequency ω_p, i.e., two photons at frequencies ω_i and ω_s combine to produce a photon at frequency ω_p (second harmonic generation is just a particular case with $\omega_s = \omega_i$). In the case of difference frequency generation two powerful beams at frequencies ω_s and ω_p interact; the beam at ω_p loses power in favor of the beam at ω_s and of the newly generated difference frequency beam at ω_i. In terms of photon balance, we can say that a photon at ω_p is split into a photon at ω_i and a photon at ω_s. Optical parametric amplification differs from difference frequency generation only in the initial conditions: in this case, in fact, the beam at ω_s (signal beam) is much weaker than that at ω_p (pump beam) and gets significantly amplified during the interaction, while at the same time the beam at ω_i (idler beam) is generated.

Neglecting pump depletion ($A_p \cong$ cost.) and assuming an initial signal intensity A_{s0} (seed beam) and no initial idler beam ($A_{i0} = 0$) Eqs. (7) can be solved to get the signal and idler intensities after a length L of nonlinear crystal

$$I_s(L) = I_{s0}\left[1 + \frac{\Gamma^2}{g^2}\sinh^2(gL)\right], \tag{9a}$$

$$I_i(L) = I_{s0}\frac{\omega_i}{\omega_s}\frac{\Gamma^2}{g^2}\sinh^2(gL), \tag{9b}$$

where

$$g = \sqrt{\Gamma^2 - \left(\frac{\Delta k}{2}\right)^2}, \tag{10}$$

$$\Gamma^2 = \frac{\omega_i \omega_s d_{\text{eff}}^2 |A_p|^2}{n_i n_s c_0^2} = \frac{2\omega_i \omega_s d_{\text{eff}}^2 I_p}{n_i n_s n_p \epsilon_0 c_0^3} = \frac{8\pi^2 d_{\text{eff}}^2 I_p}{n_i n_s n_p \lambda_i \lambda_s \epsilon_0 c_0}. \tag{11}$$

For the case of perfect phase matching ($\Delta k = 0, g = \Gamma$) and in the large gain approximation ($\Gamma L \gg 1$), Eqs. (9) simplify to

$$I_s(L) \cong \tfrac{1}{4} I_{s0} \exp(2\Gamma L), \tag{12a}$$

$$I_i(L) \cong \frac{\omega_i}{4\omega_s} I_{s0} \exp(2\Gamma L). \tag{12b}$$

Note that the ratio of signal and idler intensities is such that an equal number of signal and idler photons are generated. Equations (12) allow to define a parametric gain as

$$G = \frac{I_s(L)}{I_{s0}} = \frac{1}{4}\exp(2\Gamma L) \tag{13}$$

growing exponentially with the crystal length L and with the nonlinear coefficient Γ. Note that the exponential growth of signal and idler waves along the crystal is qualitatively different from the quadratic growth occurring in other second order nonlinear phenomena, such as sum frequency generation or second harmonic generation. This difference can be understood intuitively in the following way: in a strong pump field, the presence of a seed photon at the signal wavelength stimulates the generation of an additional signal photon and of a photon at the idler wavelength. Likewise, due to the symmetry of signal and idler, the amplification of an idler photon stimulates the generation of a signal photon. Therefore, the generation of the signal field reinforces the generation of the idler field and vice versa, giving rise to a positive feedback that is responsible for the exponential growth of the waves. Equation (11) shows that the coefficient Γ depends on: (i) the pump intensity; (ii) the signal and idler wavelengths λ_s and λ_i, (iii) the nonlinear coefficient d_{eff}; and (iv) the refractive indexes at the three interacting wavelengths. To characterize a parametric interaction and compare different nonlinear materials, it is possible to define the following figure of merit:

$$\text{FM} = \frac{d_{\text{eff}}}{\sqrt{\lambda_s \lambda_i n_p n_s n_i}}. \tag{14}$$

In the following we discuss some examples of parametric gain calculation relevant to ultrashort pulses, assuming perfect phase matching. Figure 1 shows a plot of the parametric gain in BBO, at the infrared pump wavelength $\lambda_p = 0.8\ \mu$m and the signal wavelength $\lambda_s = 1.2\ \mu$m as a function of pump intensity and for different crystal lengths. The gain scales as the exponential of the square root of the pump intensity: $G \propto \exp(\sqrt{I_p})$. At a pump intensity $I_p = 25$ GW/cm^2, a gain $G \cong 6$ is calculated for a crystal length $L = 1$ mm; however, it rapidly increases to $G \cong 2 \times 10^6$ for $L = 5$ mm. The same gain can be obtained with a 3 mm crystal increasing the pump intensity to 75 GW/cm^2. The same plot for BBO at the visible pump wavelength $\lambda_p = 0.4\ \mu$m and the signal wavelength $\lambda_s = 0.6\ \mu$m is shown in Fig. 2. In this case, at a pump intensity $I_p = 25$ GW/cm^2, a gain $G \cong 128$ is calculated for a crystal length $L = 1$ mm, about a factor of 20 larger than in the case of infrared pump. The higher gain is due to the smaller values of λ_s and λ_i, which increase the figure of merit of the parametric interaction. Despite the improvement in figure of merit using a visible pump, the group velocity

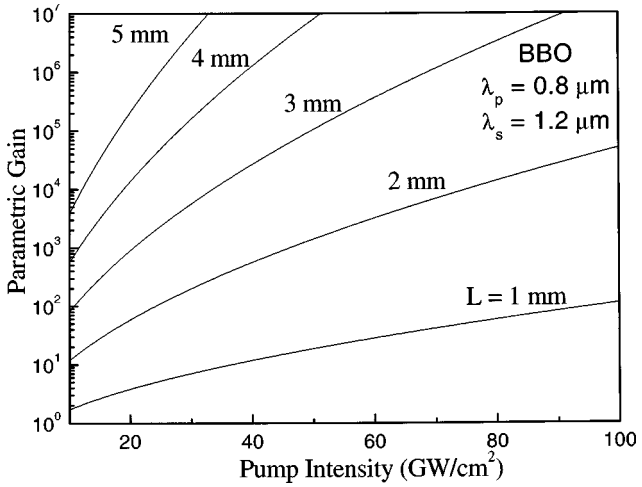

FIG. 1. Parametric gain for an OPA at the pump wavelength $\lambda_p=0.8\ \mu$m and the signal wavelength $\lambda_s=1.2\ \mu$m, using type I phase matching in BBO ($d_{\text{eff}}=2$ pm/V).

mismatch between the interacting pulses, as we will see later, prevents the use of long nonlinear crystals in this case.

We now address the problem of phase matching: to achieve maximum gain, we must satisfy the phase matching condition, $\Delta k=0$, which can be recast in the form

$$n_p=\frac{n_i\omega_i+n_s\omega_s}{\omega_p}. \tag{15}$$

It is easy to show that this condition cannot be fulfilled in bulk isotropic materials in the normal dispersion region ($n_i<n_s<n_p$). In some birefringent crystals, phase matching can be achieved by choosing for the higher frequency pump wave (ω_p) the polarization direction giving the lower refractive index. In the case, common in femtosecond OPAs, of negative uniaxial crystals ($n_e<n_o$), the pump beam is polarized along the extraordinary direction. If both signal and idler beams have the same ordinary polarization (perpendicular to that of the pump beam) we talk about type I (or $o_s+o_i\rightarrow e_p$) phase matching. If one of the two is polarized

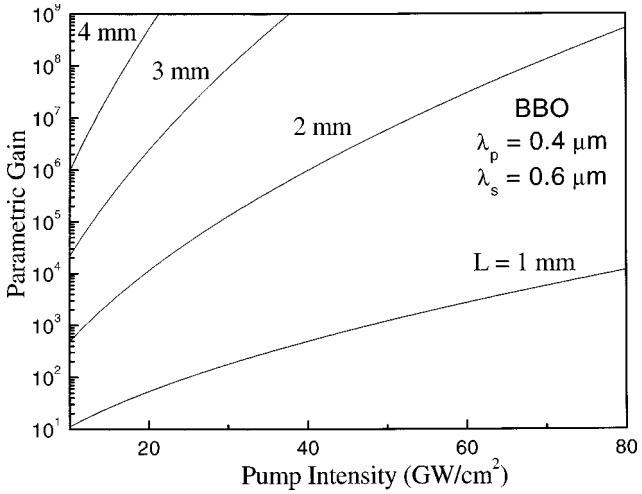

FIG. 2. Parametric gain for an OPA at the pump wavelength $\lambda_p=0.4\ \mu$m and the signal wavelength $\lambda_s=0.6\ \mu$m, using type I phase matching in BBO ($d_{\text{eff}}=2$ pm/V).

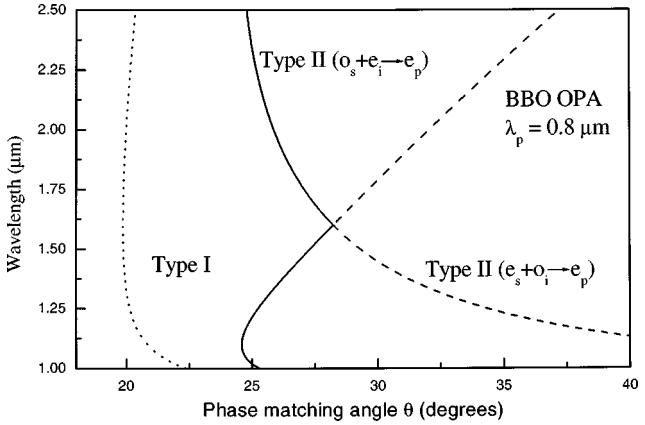

FIG. 3. Angle tuning curves for a BBO OPA at the pump wavelength $\lambda_p=0.8\ \mu$m for type I phase matching (dotted line), type II $o_s+e_i\rightarrow e_p$ phase matching (solid line), and type II $e_s+o_i\rightarrow e_p$ phase matching (dashed line).

parallel to the pump beam, we talk about type II phase matching; in this case either the signal ($e_s+o_i\rightarrow e_p$) or the idler ($o_s+e_i\rightarrow e_p$) can have the extraordinary polarization.[25] Both types of phase matching can be used and have their specific advantages according to the system under consideration. Usually the phase matching condition is achieved by adjusting the angle θ_m between the wave vector of the propagating beams and the optical axis of the nonlinear crystal (angular phase matching). Alternatively, the refractive indexes can be changed by adjusting the crystal temperature (temperature phase matching).

As an example, we consider the case of a negative uniaxial crystal, for which type I phase matching is achieved when[26]

$$n_{\text{ep}}(\theta_m)\omega_p=n_{\text{os}}\omega_s+n_{\text{oi}}\omega_i, \tag{16}$$

which allows to compute $n_{\text{ep}}(\theta_m)$. Recalling the dependence of the extraordinary index on the propagation direction in uniaxial crystals

$$\frac{1}{n_{\text{ep}}^2(\theta_m)}=\frac{\sin^2(\theta_m)}{n_{\text{ep}}^2}+\frac{\cos^2(\theta_m)}{n_{\text{op}}^2}, \tag{17}$$

where n_{ep} and n_{op} are the principal extraordinary and ordinary refractive indexes at the pump wavelength, the phase matching angle can then be obtained as

$$\theta_m=\text{asin}\left[\frac{n_{\text{ep}}}{n_{\text{ep}}(\theta_m)}\sqrt{\frac{n_{\text{op}}^2-n_{\text{ep}}^2(\theta_m)}{n_{\text{op}}^2-n_{\text{ep}}^2}}\right]. \tag{18}$$

Figures 3 and 4 show the phase matching angles as a function of wavelength for BBO types I and II OPAs at the pump wavelengths 0.8 and 0.4 μm. Note that, in general, the phase matching angle shows a less pronounced wavelength dependence for type I with respect to type II phase matching.

B. Parametric amplification with ultrashort pulses

So far we have studied the interaction of three monochromatic waves, i.e., cw beams. Let us now consider the case, relevant for femtosecond OPAs, of three pulses like

$$E(z,t)=\text{Re}\{A(z,t)\exp[j(\omega t-kz)]\} \tag{19}$$

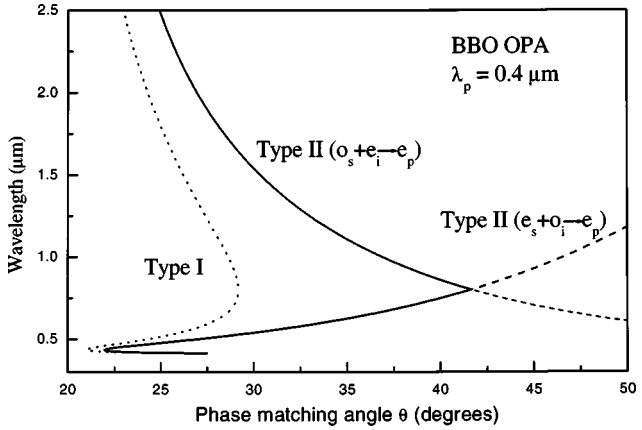

FIG. 4. Angle tuning curves for a BBO OPA at the pump wavelength $\lambda_p = 0.4\ \mu$m for type I phase matching (dotted line), type II $o_s+e_i \rightarrow e_p$ phase matching (solid line), and type II $e_s+o_i \rightarrow e_p$ phase matching (dashed line).

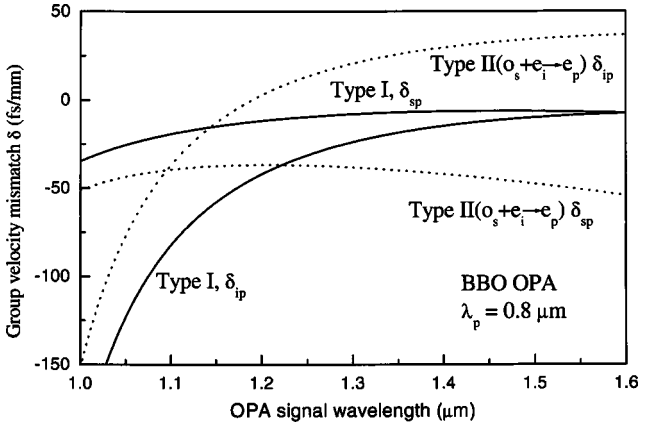

FIG. 5. Pump-signal (δ_{sp}) and pump-idler (δ_{ip}) group velocity mismatch curves for a BBO OPA at the pump wavelength $\lambda_p = 0.8\ \mu$m for type I phase matching (solid line) and type II $o_s+e_i \rightarrow e_p$ phase matching (dashed line).

propagating in the nonlinear crystal with different group velocities $\nu_g = d\omega/dk$. Within the slowly varying amplitude approximation and neglecting pulse lengthening due to second or higher order dispersion (which is a good approximation for pulses in the 100 fs range), we obtain the following equations:[27,28]

$$\frac{\partial A_s}{\partial z}+\frac{1}{\nu_{gs}}\frac{\partial A_s}{\partial t}=-j\frac{\omega_s d_{\text{eff}}}{n_s c_0}A_i^* A_p \exp(-j\Delta kz), \tag{20a}$$

$$\frac{\partial A_i}{\partial z}+\frac{1}{\nu_{gi}}\frac{\partial A_i}{\partial t}=-j\frac{\omega_i d_{\text{eff}}}{n_i c_0}A_s^* A_p \exp(-j\Delta kz), \tag{20b}$$

$$\frac{\partial A_p}{\partial z}+\frac{1}{\nu_{gp}}\frac{\partial A_p}{\partial t}=-j\frac{\omega_p d_{\text{eff}}}{n_p c_0}A_s A_i \exp(+j\Delta kz). \tag{20c}$$

Note that Eqs. (20) neglect also third order nonlinear effects (self- and cross-phase modulation). By transforming to a frame of reference that is moving with the group velocity of the pump pulse ($\tau = t - z/\nu_{gp}$) we obtain the equations

$$\frac{\partial A_s}{\partial z}+\left(\frac{1}{\nu_{gs}}-\frac{1}{\nu_{gp}}\right)\frac{\partial A_s}{\partial \tau}=-j\frac{\omega_s d_{\text{eff}}}{n_s c_0}A_i^* A_p \exp(-j\Delta kz), \tag{21a}$$

$$\frac{\partial A_i}{\partial z}+\left(\frac{1}{\nu_{gi}}-\frac{1}{\nu_{gp}}\right)\frac{\partial A_i}{\partial \tau}=-j\frac{\omega_i d_{\text{eff}}}{n_i c_0}A_s^* A_p \exp[-j\Delta kz], \tag{21b}$$

$$\frac{\partial A_p}{\partial z}=-j\frac{\omega_p d_{\text{eff}}}{n_p c_0}A_s A_i \exp(j\Delta kz). \tag{21c}$$

Despite the many simplifications, Eqs. (21) capture the main issues of parametric amplification with ultrashort pulses, that are related to group velocity mismatch (GVM) between the interacting pulses. In particular, GVM between the pump and the amplified (signal and idler) pulses limits the interaction length over which parametric amplification takes place, while GVM between the signal and the idler beams limits the phase matching bandwidth.

The useful interaction length for parametric interaction is quantified by the pulse splitting length, which is defined as the propagation length after which the signal (or the idler) pulse separates from the pump pulse in the absence of gain, and is expressed as

$$\ell_{\text{jp}} = \frac{\tau}{\delta_{\text{jp}}}, \quad j = s, i, \tag{22}$$

where τ is the pump pulse duration and $\delta_{\text{jp}} = 1/\nu_{\text{gj}} - 1/\nu_{\text{gp}}$ is the GVM between pump and signal/idler. Note that the pulse splitting length becomes shorter for decreasing pulse duration and for increasing GVM. GVM depends on the crystal type, pump wavelength, and type of phase matching. Figures 5 and 6 show examples of GVM curves for a BBO OPA pumped by 0.8 and 0.4 μm pulses, respectively. Note that, due to greater dispersion values in the visible, GVM is in general larger in this wavelength range.

For crystal lengths shorter than the pulse splitting length, GVM effects can be neglected, to a first approximation, and Eqs. (9)–(12), valid for cw beams, can be used for gain calculations. For crystals longer than or comparable to the pulse splitting length, GVM plays a crucial role and Eqs. (21) must be solved numerically to properly account for it. There is a qualitatively significant difference between the cases in which δ_{sp} and δ_{ip} have the same or different signs.

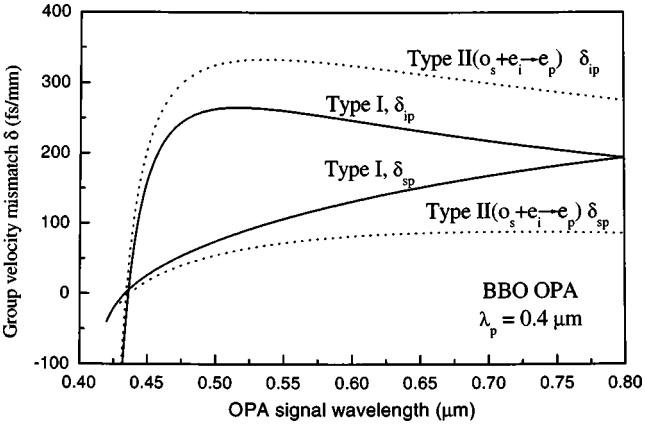

FIG. 6. Pump-signal (δ_{sp}) and pump-idler (δ_{ip}) group velocity mismatch curves for a BBO OPA at the pump wavelength $\lambda_p = 0.4\ \mu$m for type I phase matching (solid line) and type II $o_s+e_i \rightarrow e_p$ phase matching (dashed line).

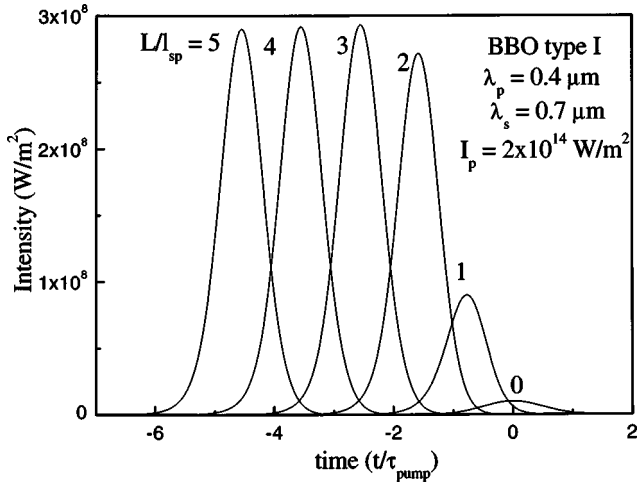

FIG. 7. Signal pulse evolution for a BBO type I OPA with $\lambda_p=0.4\ \mu$m, $\lambda_s=0.7\ \mu$m, for different lengths L of the nonlinear crystal. Pump intensity is 20 GW/cm^2. Time is normalized to the pump pulse duration and the crystal length to the pump-signal pulse splitting length.

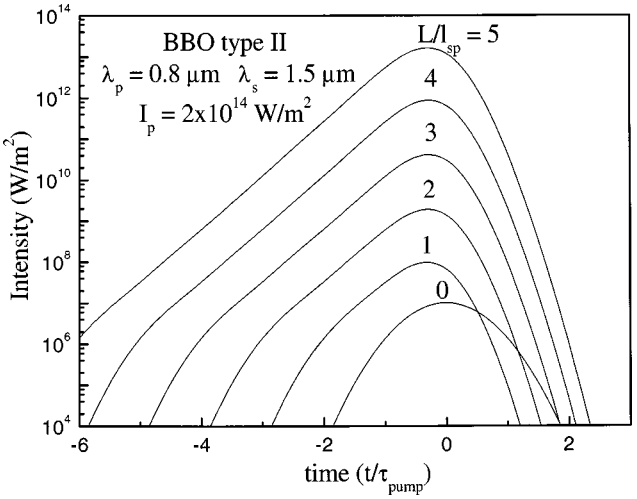

FIG. 8. Signal pulse evolution for a BBO type II OPA with $\lambda_p=0.8\ \mu$m, $\lambda_s=1.5\ \mu$m, for different lengths L of the nonlinear crystal. Pump intensity is 20 GW/cm^2. Time is normalized to the pump pulse duration and the crystal length to the pump-signal pulse splitting length.

When $\delta_{sp}\delta_{ip}>0$, both the signal and the idler pulses walk away from the pump in the same direction so that the gain rapidly decreases for propagation distances longer than the pulse splitting length and eventually saturates. On the other hand, when $\delta_{sp}\delta_{ip}<0$ signal and idler pulses move in opposite direction with respect to the pump; in this way the signal and idler pulses tend to stay localized under the pump pulse and the gain grows exponentially even for crystal lengths well in excess of the pulse splitting length. To try to rationalize this effect, we can consider the situation in which the signal pulse has moved slightly to the left and the idler pulse to the right of the pump pulse: during the parametric process, the signal pulse generates idler photons, which move to the right, i.e., towards the peak of the pump; on the other hand the idler pulse will generate signal photons which in turn move to the left, again towards the peak of the pump. This concentration of photons under the peak of the pump explains the exponential gain growth. In Fig. 7 we show an example of solution of Eqs. (21) for the case $\delta_{sp}\delta_{ip}>0$; we consider a type I BBO OPA pumped at 0.4 μm with signal wavelength $\lambda_s=0.7\ \mu$m, with GVMs $\delta_{sp}=167$ fs/mm and $\delta_{ip}=220$ fs/mm. We see that, after an initial growth, the gain rapidly tends to saturate because both signal and idler pulses temporally separate from the pump. Note that, because the trailing edge of the pulse resides for a longer time in the amplification region, there is a modest pulse shortening (20%–30%) and asymmetry. The case $\delta_{sp}\delta_{ip}<0$ is shown in Fig. 8; we consider a type II BBO OPA pumped at 0.8 μm with signal wavelength $\lambda_s=1.5\ \mu$m, having group velocity mismatches $\delta_{ip}=-47.5$ fs/mm and $\delta_{sp}=34.6$ fs/mm. Here we see that the signal growth stays exponential for propagation distances well exceeding the pulse splitting length and that the signal pulse tends to stay localized under the pump.

In the following we will show that GVM between signal and idler pulses determines the phase matching bandwidth for the parametric amplification process. Let us assume that perfect phase matching is achieved for a given signal frequency ω_s (and for the corresponding idler frequency $\omega_i=\omega_p-\omega_s$). If the signal frequency increases to $\omega_s+\Delta\omega$, by energy conservation the idler frequency decreases to $\omega_i-\Delta\omega$. The wave vector mismatch can then be approximated to the first order as

$$\Delta k\cong-\frac{\partial k_s}{\partial\omega_s}\Delta\omega+\frac{\partial k_i}{\partial\omega_i}\Delta\omega=\left(\frac{1}{\nu_{gi}}-\frac{1}{\nu_{gs}}\right)\Delta\omega. \tag{23}$$

The full width at half maximum (FWHM) phase matching bandwidth can then, within the large-gain approximation, be calculated as

$$\Delta\nu\cong\frac{2(\ln 2)^{1/2}}{\pi}\left(\frac{\Gamma}{L}\right)^{1/2}\frac{1}{\left|\dfrac{1}{\nu_{gs}}-\dfrac{1}{\nu_{gi}}\right|}. \tag{24}$$

Large GVM between signal and idler waves dramatically decreases the phase matching bandwidth; large gain bandwidth can be expected when the OPA approaches degeneracy ($\omega_s\rightarrow\omega_i$) in type I phase matching or in the case of group-velocity matching between signal and idler ($\nu_{gs}=\nu_{gi}$). Obviously, in this case Eq. (24) loses validity and the phase mismatch Δk must be expanded to the second order, giving

$$\Delta\nu=2\frac{(\ln 2)^{1/4}}{\pi}\left(\frac{\Gamma}{L}\right)^{1/4}\frac{1}{\left|\dfrac{\partial^2 k_s}{\partial\omega_s^2}+\dfrac{\partial^2 k_i}{\partial\omega_i^2}\right|}. \tag{25}$$

Figures 9 and 10 show typical plots of phase matching bandwidths for BBO OPAs, pumped at 0.8 and 0.4 μm, respectively. We see a remarkable difference between types I and II phase matching: for type II interaction, the bandwidth is smaller than in type I and stays more or less constant over the tuning range, while for type I interaction, as previously said, the bandwidth increases as the OPA approaches degeneracy. These features can be exploited for different applications: type I phase matching is used to achieve the shortest pulses, while type II phase matching allows to obtain relatively narrow bandwidths over broad tuning ranges, which are required for many spectroscopic investigations.

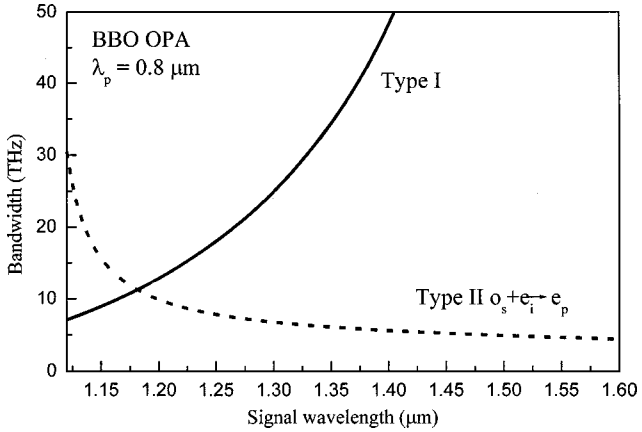

FIG. 9. Phase matching bandwidth for a BBO OPA at the pump wavelength $\lambda_p = 0.8\ \mu$m for type I phase matching (solid line) and type II $o_s + e_i \rightarrow e_p$ phase matching (dashed line). Crystal length is 4 mm and pump intensity 50 GW/cm^2.

So far we have only considered a collinear interaction, in which, once the phase matching condition ($\Delta k = 0$) is achieved, the group velocities of signal and idler, and thus the phase matching bandwidth, are set. In Sec. IV we will see that in a noncollinear interaction there is an additional degree of freedom, the pump-signal angle α. Suitably selecting this angle, it is often possible to achieve simultaneously phase matching and group velocity matching between signal and idler, thus obtaining very broad gain bandwidths.

III. OPTICAL PARAMETRIC AMPLIFIER DESIGNS

Although a great variety of femtosecond optical parametric amplifier designs have been reported, there are a few basic principles underlying the different implementations. Before illustrating in detail some of the most common OPA designs, we will try to present a very general description of the operating principles of an OPA, according to the scheme shown in Fig. 11. Femtosecond OPAs are in general pumped by amplified Ti:sapphire lasers: standard systems typically run at 1 kHz repetition rate and generate pulses at the wavelength $\lambda \cong 0.8\ \mu$m, with 0.5–1 mJ energy and duration ranging from 50 to 150 fs. Other work has reported OPAs pumped by systems running at much higher repetition rate (up to 250 kHz) but with much lower pulse energy (5–10 μJ).[29] Pumping can take place at the FW or at the SH of the Ti:sapphire laser (i.e., 800 or 400 nm). Since the optical parametric amplification process consists of the interaction of a weak signal beam with a strong pump beam, the first stage of any OPA system is the generation of the initial signal beam, the so-called seed beam. Since the seed beam is at a different frequency from the pump beam, a nonlinear optical process is required for its generation. Two different techniques have been used for the seed generation: parametric superfluorescence and white-light continuum generation.

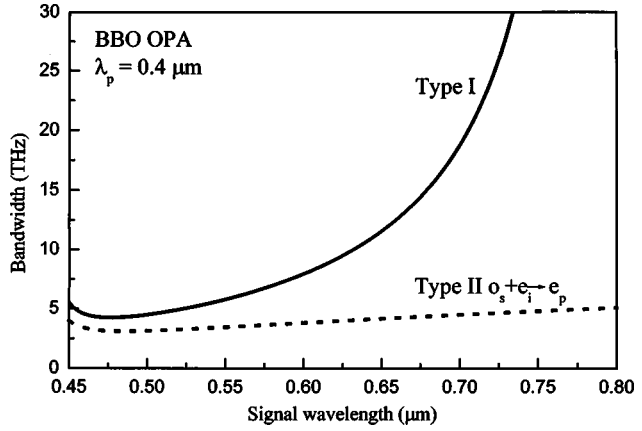

FIG. 10. Phase matching bandwidth for a BBO OPA at the pump wavelength $\lambda_p = 0.4\ \mu$m for type I phase matching (solid line) and type II $o_s + e_i \rightarrow e_p$ phase matching (dashed line). Crystal length is 2 mm and pump intensity 100 GW/cm^2.

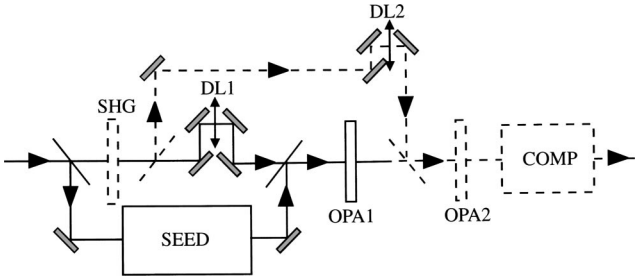

FIG. 11. Scheme of an ultrafast optical parametric amplifier. SEED: seed generation stage; DL1, DL2: delay lines; OPA1, OPA2 parametric amplification stages; COMP: compressor.

Parametric superfluorescence[18,30] is a parametric amplification of the vacuum or quantum noise, and can be also thought as two-photon spontaneous emission from a virtual level excited by the pump field. In practice it is simply achieved by pumping a suitable nonlinear crystal, which is often of the same types as the ones used in the subsequent OPA stages; amplification will occur at those wavelengths for which the parametric interaction is phase matched. The advantage of parametric superfluorescence is the possibility of achieving large amplification and substantial seed pulse energies; its disadvantages are the inherent fluctuations of a process starting from quantum noise, and the poor spatial quality of the generated seed beam.

White light generation[31,32] occurs when an intense ultrashort pulse is focused inside a transparent material, such as fused silica or sapphire: as a result of the interplay between self-focusing and self-phase modulation, a large spectral broadening takes place. Although the processes occurring during the generation of white-light continuum are still not fully understood,[33] its properties are very good for its use as an OPA seed. When focusing 0.8 μm, 100 fs pulses into a sapphire plate, with thickness ranging from 1 to 3 mm, the threshold for white-light generation is around 1 μJ. (The exact value depends on the focusing conditions.) The continuum spectrum extends throughout the visible (down to $\approx$0.42 μm) and the near-IR (up to $\approx$1.5 μm), with an energy of approximately 10 pJ per nm of bandwidth. Under the correct conditions (i.e., a single self-focused filament) the white light has an excellent spatial quality, with a circular gaussian beam, and a very high pulse-to-pulse stability. When using materials with high thermal conductivity and low UV absorption such as sapphire, no long-term degradation of the material is experienced.

Following generation of the seed pulse, the pump and seed pulses are combined in a suitable nonlinear crystal, in a first parametric amplification stage (preamplifier). To achieve temporal overlap, their relative timing must be adjusted by a delay line. Often the pump spot size in the nonlinear crystal is set by a telescope and is chosen to achieve the highest possible gain without causing optical damage of the crystal, or inducing third-order nonlinear effects (self-focusing, self-phase modulation, or white light generation) that would cause beam distortion or breakup. In case of parametric superfluorescence seed, the preamplifier is also used as a spatial filter, to improve the spatial coherence of the signal beam by amplifying only those spatial components of the superfluorescence that overlap the pump beam in the crystal. After the first amplification stage, the signal beam can be further amplified in a second stage, power amplifier. Usually this stage is driven into saturation, i.e., with significant pump depletion and conversion efficiency above 30%. In this regime, the amplified energy is less sensitive to seed fluctuations, and high pulse stability can be achieved. The purpose of using two amplification stages instead of one long crystal is twofold: (i) the GVM between pump and signal pulses in the first stage can be compensated by a delay line; and (ii) this scheme gives the flexibility of separately adjusting the pump intensity, and thus the parametric gain, in the two stages. After the power amplifier, signal and idler beams are separated from the pump and from each other using dichroic filters or mirrors. Finally, in case of broadband amplification, a pulse compressor is used to obtain transform-limited pulse duration.

We will now review the state of art in OPA design in different spectral ranges.

A. OPA in the near-IR

OPAs tunable in the near-IR, pumped by the fundamental (800 nm) radiation of an amplified Ti:sapphire laser, are the most straightforward to operate.[34–45] They have the following advantages: (i) high available pump energies (up to the millijoule level); and (ii) low pump-signal and pump-idler GVM values. Low GVM allows the use of long nonlinear crystals, making it possible to obtain high gains. These advantages are partially offset by a lower figure of merit for the parametric interaction in the near-IR compared to the visible. Tunability is limited by the losses due to absorption of the idler wave in the nonlinear crystal. This is typically a problem at wavelengths longer than ≈ 3 μm. Therefore, the signal beam is tunable from degeneracy (1.6 μm) to 1.1 μm while the idler beam tunes from 1.6 to 3 μm. There is, however, a ''hole'' in the tuning range from 0.8 to 1.1 μm.

Most systems use BBO as nonlinear crystal, because of its high nonlinearity and favorable dispersion properties. As can be seen from Fig. 5, pump-signal and pump-idler GVM values are quite low in the case of type I phase matching, so that, for 100 fs pump pulses, pump-signal temporal overlap can be maintained for crystal lengths up to ≈ 7 mm. On the other hand, with type II phase matching pump-signal and pump-idler GVMs have opposite signs so that, as explained in the discussion in Sec. II B, exponential growth of the gain is preserved for crystal lengths well in excess of the pulse splitting length. Other advantages of type II phase matching are a phase matching bandwidth that is relatively constant over most of the tuning range and the possibility to separate signal and idler pulses because of their orthogonal polarization. This last point is especially important when operating the OPA close to degeneracy, where these wavelengths are quite close to each other. A typical setup for a white-light seeded near-IR OPA is shown in Fig. 12;[44] the OPA is pumped by an amplified Ti:sapphire laser generating ≈ 500 μJ, 50 fs pulses at 1 kHz repetition rate. A small fraction of the pump light (≈ 2 μJ) is used to generate the white-light seed in a 2-mm-thick sapphire plate; the near-IR fraction of the continuum is amplified in a first stage consisting of a 3 mm long BBO crystal cut for type II phase matching ($\theta = 28°$). Pumping with ≈ 50 μJ of energy, up to 6 μJ energy at the signal wavelength is obtained. Wavelength tuning is achieved by changing the phase matching angle of the crystal and simultaneously optimizing the pump-seed delay. The second stage consists of an identical BBO crystal pumped by ≈ 450 μJ of energy, and generates up to 200 μJ of amplified signal light, corresponding to a conversion efficiency of 45%; the pulse width ranges from 30 to 50 fs across the tuning range. Similar results in terms of pulse energies are obtained using a parametric superfluorescence seed;[42] in this case, significant compression of the signal pulse (60 fs) with respect to the pump pulse (150 fs) is observed, due to the nonlinear effects taking place in the parametric process at high conversion efficiencies.

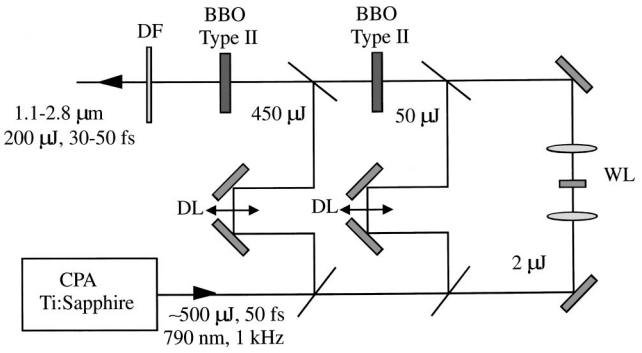

FIG. 12. Scheme of a near-IR OPA DL: delay lines; WL: white light generation stage; DF: dichroic filter.

B. OPA in the visible

The generation of femtosecond pulses tunable in the visible is important for a variety of spectroscopic applications, because many systems of interest in physics, chemistry, and biology have absorption bands in this range. A straightforward way of achieving tunable visible pulses consists in frequency doubling the output of an 0.8 μm pumped near-IR OPA;[43,46] however, since absorption of the idler in the nonlinear crystal sets a blue tuning limit of ≈ 1.1 μm, the SH would be tunable down to only 0.55 μm, leaving a substantial part of the visible range uncovered. Pumping with the SH of a Ti:sapphire laser around 0.4 μm, the signal can be tuned through most of the visible range, from ≈ 0.45 μm to degeneracy (0.8 μm). Correspondingly, the idler tunes from 0.8 to 2.5 μm; this fills the gap in the tuning range for near-IR

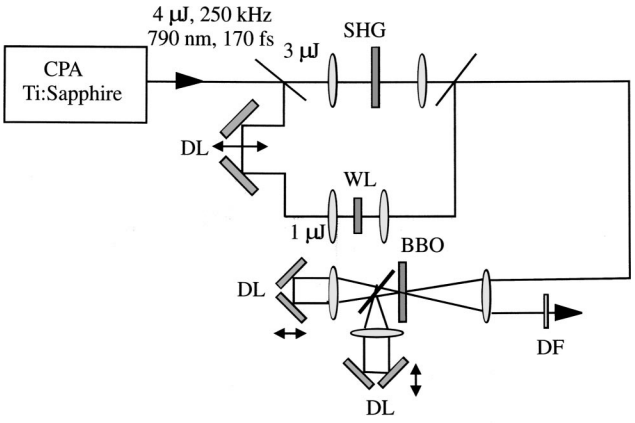

FIG. 13. Scheme of a visible OPA. DL: delay lines; WL: white light generation stage; SHG: second harmonic generation stage; DF: dichroic filter.

OPAs.[47–62] Visible OPAs in general obtain lower energies than near-IR ones, because of the lower pump energy available from a frequency doubled pump. Furthermore GVM is much larger in the visible range (see Fig. 6), which limits the use of long nonlinear crystals. This disadvantage is partially compensated for by the larger figures of merit for parametric interaction in the visible. Also for visible OPAs the most popular nonlinear material is BBO. Type II phase matching provides gain bandwidths that are narrower and stay essentially constant over the tuning range, which may be beneficial for some spectroscopic applications.[52]

Figure 13 shows a typical visible OPA design;[49–51] the system is pumped by an high repetition rate amplified Ti:sapphire laser, generating 4 μJ, 170 fs pulses at 250 kHz repetition rate. A fraction of the beam is used to generate a white-light seed in a 3-mm-thick sapphire plate, while the remaining part is frequency doubled in a BBO crystal to give 1 μJ of energy at 0.4 μm; the pump and seed beams are then combined by a dichroic mirror and their path lengths are matched by a suitable delay line. The two pulses are then focused on a 1-mm-thick BBO OPA crystal, cut for type I phase matching; the crystal thickness is close to the pump-signal pulse splitting length for BBO in the visible (see Fig. 6). The white-light seed component to be amplified is selected by simply rotating the BBO crystal and reoptimizing the pump-seed delay in order to compensate for the group velocity dispersion in the continuum. Given the small crystal thickness, high pump intensities are required to achieve high parametric gain; in this design intensities lower than 50 GW/cm^2 are used to avoid the onset of self-focusing effects in the BBO crystal. Typical single-pass gains in this system are in the order of 100. The BBO crystal is placed after the focus of the lens, i.e., in a diverging beam. This technique makes it possible to prevent self-focusing and use higher intensities than would be possible by just putting the crystal at the focus of a longer-focal-length lens. After the first pass, pump and signal beams are separated by a dichroic beam splitter, and then reflected back into the BBO OPA crystal for a second amplification pass. Two passes in the crystal, instead of a single pass in a crystal of double length, are required to compensate for the GVM effects by suitably adjusting the delays. Typical gains in the second pass are around 10, giving signal energies of $\approx$150 nJ, which represent a 15% conversion efficiency of the pump pulse energy. After amplification, the signal beam is collimated and separated from the remaining pump and idler beams by dichroic reflectors. The amplified pulses are tunable, in the visible, from 0.47 μm to beyond 0.7 μm; they display excellent spatial quality and peak-to-peak noise less than 5% across the entire tuning range. Because of type I phase matching, the amplified pulse bandwidth strongly depends on signal wavelength (see Fig. 10), increasing in the red as degeneracy is approached. The pulses generated by the OPA are not transform limited, but are frequency chirped by the white-light generation process and by group velocity dispersion in the optics and the BBO crystal. This chirp can be removed with a prism compressor and transform-limited pulses are generated, with duration ranging from 80 fs in the blue to less than 30 fs in the red; note that the OPA generates pulses that are considerably shorter than the pump pulses. The limitation in achievable pulsewidth is set by the relatively narrow phase matching bandwidths available in a collinear interaction geometry. A possible solution to this problem consists of changing the phase-matching angle in the subsequent amplification stage, so as to amplify at each pass a different spectral region of the white light;[59] this technique makes it possible to generate 30 fs pulses tunable throughout the visible. A more effective solution to the problem, which consists in using a non-collinear interaction geometry, will be discussed in Sec. IV.

C. OPA in the mid-IR

The generation of tunable femtosecond pulses in the mid-IR spectral region is very interesting for several spectroscopic applications, such as study of vibrational transitions in molecules or intersubband transitions in semiconductor nanostructures; therefore several approaches have been developed to generate pulses in this wavelength range.

Mid-IR pulses can be obtained from the idler of a 0.8 μm pumped OPA; however, in the most commonly used crystal, BBO, tuning is limited to wavelengths shorter than 3 μm by the onset of IR absorption. The tuning range can be extended up to wavelengths longer than 4 μm, with output energies in the microjoule range, by using different nonlinear crystals, such as $KTiOPO_4$ or its isomorphs,[63,64] $KNbO_3$,[65] or $MgO:LiNbO_3$.[66] For these systems, the efficiency can be increased and the temporal and spectral quality of the OPA pulses can be preserved by seeding the OPA, at the signal wavelength, with a narrow-band nanosecond pulse (often derived from the pump laser of the regenerative amplifier).[67] However, the tuning range in these systems is limited to $\approx$5 μm not only by the long-wavelength transparency cutoff but also by the increasing GVM between the signal and idler beams. Nonlinear crystals with extended mid-IR transparency range are available, but the pumping wavelength needs to be tuned to the infrared, because of residual absorption or lack of phase matching at 0.8 μm. In $ZnGeP_2$, pumped at 2 μm by the idler beam of a 0.8 μm pumped OPA, tuning from 2.5 to 10 μm was demonstrated;[68] more recently, a mercury thiogallate ($HgGa_2S_4$) OPA, pumped at 1.25 μm by an am-

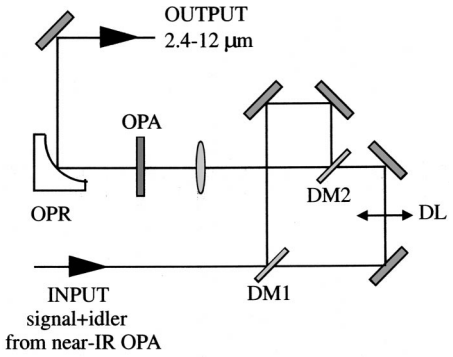

FIG. 14. Scheme of a mid-IR pulse generation stage. DM1, DM2, dichroic mirrors; DL: delay line; OPR: off-axis parabolic reflector.

plified Cr:forsterite system, showed tunability from 5 to 9 μm with microjoule-level output energy and pulse duration below 200 fs.[69]

An alternative way to generate tunable mid-IR pulses is by difference-frequency generation (DFG) between the signal and the idler pulses of a 0.8 μm pumped OPA. The most commonly used crystal in this case is $AgGaS_2$, which allows continuous tuning from 2.4 μm to wavelengths longer than 12 μm;[70] in this case, the output energies are in the tens of nanojoule range, significantly lower than with previous implementations, however repetition rates up to 250 kHz have been demonstrated.[71,72] A typical setup for DFG is shown in Fig. 14: the collinear signal and idler beams are generated by a near-IR type II OPA and have thus perpendicular polarization, as is required for phase matching in the DFG process. The two pulses are separated by a dichroic mirror, reflecting the signal and transmitting the idler, so that their relative delay can be adjusted, and then recombined using an identical mirror. The two collinear pulses are then focused by a quartz lens onto a 1-mm-thick $AgGaS_2$ crystal, cut for type II phase matching ($\theta=40°$). After the crystal, standard lenses cannot be used to collimate the DFG signal, because of their absorption bands in the mid-IR; an inexpensive alternative for collimating and focussing mid-IR wavelengths is a diamond-turned, off-axis parabola. A similar, alternative method for generation of mid-IR pulses consists in difference frequency mixing of the output of a single-cavity, two-color femtosecond Ti:sapphire laser.[73]

An even simpler technique for the generation of tunable mid-IR pulses consists of optical rectification of a single ultrashort pulse focused in a suitable electro-optic material. This technique has been initially used for the generation of far-IR radiation, with a frequency of a few tetrahertz[74–76] which was in turn detected by electro-optic sampling;[77] it has been subsequently extended to the mid-IR frequency range.[78–81] Using a very short excitation pulse (with duration of 20 fs or less) it is possible to obtain tunable mid-IR pulses by difference-frequency generation of different spectral components of a broadband pulse spectrum. In this case a single ultrashort pulse is required generated directly from a femtosecond oscillator (possibly cavity dumped or amplified) or by external pulse compression:[82] by varying the phase matching angle of the nonlinear crystal (GaAs or GaSe), the center wavelength of the difference frequency pulse can be continuously tuned from 7 to 20 μm, with pulse duration in the 100 fs range.

D. OPA in the ultraviolet

The generation of ultrashort laser pulses tunable in the UV spectral range, especially in the extreme-ultraviolet (XUV) region, is important for spectroscopic investigations and also for technological applications, such as for example photolithography. A straightforward way of achieving tunable UV pulses consists in frequency doubling[83] or upconverting with a powerful IR pulse[84] the output of a visible OPA: these arrangements result in pulses with 100 nJ level energy, 30–50 fs duration and tunability from 0.25 to 0.35 μm. Even shorter wavelengths can be obtained by using nonlinear crystals with extended UV transparency, such as cesium lithium borate.[85] To achieve even shorter wavelengths and develop a true UV OPA, two obvious problems need to be addressed: (i) finding a nonlinear medium that is transparent at UV wavelengths; and (ii) finding a suitable pump laser at UV wavelengths. The first problem can be solved by using, as nonlinear medium, a gas or a plasma, while pumping can occur at IR or visible wavelengths exploiting a multiphoton process. This scheme, called high-order optical parametric amplification (HOPA),[86–92] generates signal and idler waves via the process

$$q\hbar\omega_p=\hbar\omega_i+\hbar\omega_s, \tag{26}$$

where q is an integer. In this case the equations describing the parametric interaction, in the undepleted pump approximation, can be written as

$$\frac{dA_i}{dz}=-j\frac{\pi\omega_i}{n_ic_0}\frac{q+1}{2^{q-1}}N\chi^{(q+1)}(\omega_i)A_s^*A_p^q\exp(-j\Delta kz), \tag{27a}$$

$$\frac{dA_s}{dz}=-j\frac{\pi\omega_s}{n_sc_0}\frac{q+1}{2^{q-1}}N\chi^{(q+1)}(\omega_s)A_i^*A_p^q\exp(-j\Delta kz), \tag{27b}$$

where $\Delta k=qk_p-k_s-k_i$ is the wave vector mismatch, N is the atomic density, and $\chi^{(q+1)}(\omega_s)$, $\chi^{(q+1)}(\omega_i)$ are the nonlinear atomic susceptibilities for the q-order process, which can be assumed as equal if sufficiently far from resonances. Equations (27) bear similarity to Eqs. (7), describing parametric amplification in a second-order medium and have analogous solutions giving, in the large-gain limit, exponential growth of signal and idler waves along the propagation direction. In particular, it is possible to define a gain coefficient as

$$\Gamma=\frac{\pi}{c}\left(\frac{\omega_s\omega_i}{n_sn_i}\right)^2\frac{q+1}{2^{q-1}}N\chi^{(q+1)}|A_p|^q. \tag{28}$$

This coefficient is much smaller than in ordinary OPAs, because of the lower nonlinear susceptibilities associated to multiphoton processes, which can be enhanced by adjusting the pump frequency close to a q-photon resonance of the medium. The HOPA is seeded by the idler beam, which is chosen in the visible (or infrared) frequency range, so that

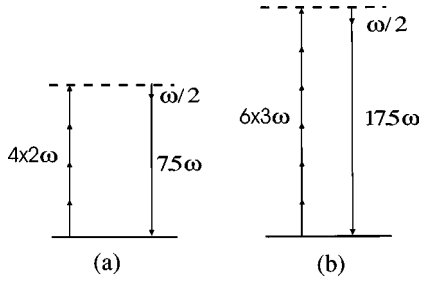

FIG. 15. Phase-matching schemes for HOPAs in a plasma.

the signal is in the UV range. Given the low gain coefficients, to achieve significant amplification it is necessary to satisfy the phase-matching condition $\Delta k=0$.

The first experimental demonstration of the HOPA concept was obtained by Durfee *et al.*,[86,87] who generated the third harmonic of a Ti:sapphire laser by the parametric process $2\times 2\omega=\omega+3\omega$. The experiments were performed in a gas filled hollow core fiber, which has the advantage of greatly extending the interaction length. In addition, the hollow fiber provides a simple way of obtaining phase matching. In this structure, in fact, phase mismatch between the different propagating waves results from a combination of modal dispersion, depending on the propagating modes and the fiber diameter, and material dispersion, depending on the gas pressure. If the modes of the interacting waves are selected in such way that the two dispersions have opposite sign, phase matching can be achieved by simply tuning the gas pressure. In these initial experiments, both the fundamental and the SH of the Ti:sapphire laser are injected in the hollow core fiber: pulses at the third harmonic with energy in excess of 1 μJ and 8 fs duration were obtained. Recently, this technique was extended to the generation of the fourth and fifth harmonic of the Ti:sapphire laser.[88] Phase matched high-order difference frequency mixing for the ninth harmonic of Ti:sapphire was achieved in a plasma, driven by the fundamental and the SH, according to the process $6\times 2\omega-3\omega=9\omega$.[93]

Another elegant proposal for achieving phase matching consists in using as nonlinear medium a plasma, for which the refractive index is essentially determined by the free electrons, and its frequency dependence can be approximated as

$$n(\omega)\cong 1-\frac{\omega_{\mathrm{pl}}^2}{\omega^2}, \tag{29}$$

ω_{pl} being the plasma frequency. If the condition $\omega_s \gg \omega_{\mathrm{pl}}$ is satisfied, then $n(\omega_s)\cong 1$ and the phase-matching condition becomes

$$q\omega_p[n(\omega_p)-1]=\omega_i[n(\omega_i)-1]. \tag{30}$$

By using Eq. (29), it is straightforward to show that Eq. (30) is satisfied when $\omega_i=\omega_p/q$. Two possible schemes of phase-matched HOPA in a plasma are shown in Fig. 15. In case (b), for example, the pump beam at $\omega_p=3\omega$ is provided by the third harmonic of a Ti:sapphire laser, while the idler beam at $\omega_i=\omega/2$ is generated by an IR OPA tuned to degeneracy; amplification is obtained at $\omega_s=17.5\omega$, well within the XUV range.

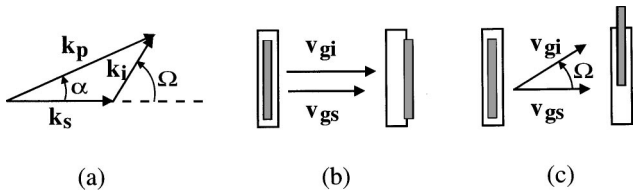

FIG. 16. (a) Schematic of a noncollinear interaction geometry; (b) representation of signal and idler pulses in the case of collinear interaction; and (c) same as (b) for noncollinear interaction.

Finally, a method for generating UV radiation is high harmonic generation (HHG) from a noble gas[94,95] exposed to an ultrashort pulse. While the HHG radiation is at odd harmonics of the driver laser frequency, tunability can be achieved by either using an OPA to generate the harmonics or mixing, in the gas, radiation from an high energy, fixed frequency source and a tunable OPA.[96,97]

IV. ULTRABROADBAND OPTICAL PARAMETRIC AMPLIFIERS

Until recently the shortest pulses achieved from OPAs have been in the 30–50 fs range, limited either by the narrow phase matching bandwidths or by the long pump pulse duration. In the following we report on different OPA schemes which overcome these difficulties and generate few-optical-cycle pulses with microjoule-level energy in the visible as well as in the infrared. In the visible, relatively long pump pulses ($\approx$100 fs) are used and the properties of noncollinear phase matching are exploited to achieve broadband amplification of the white-light seed; the amplified pulses are then compressed to sub-10 fs duration using suitable dispersive delay lines. In the infrared, ultrabroadband pulses can be generated using short (20–40 fs) pump pulses and exploiting nonlinear compression effects arising in the parametric amplification process at high conversion efficiencies.

A. Noncollinear visible optical parametric amplifier

In an OPA using a collinear interaction geometry, the propagation direction in the nonlinear crystal is selected to satisfy, for a given signal wavelength, the phase-matching condition $\Delta k=0$. In this condition the signal and idler group velocities are fixed and so the phase matching bandwidth of the process [see Eq. (24)]. An additional degree of freedom can be introduced using a noncollinear geometry, such as that shown in Fig. 16(a): pump and signal wave vectors form an angle α (independent of signal wavelength) and the idler is emitted at an angle Ω with respect to the signal. In this case the phase matching condition becomes a vector equation, which, projected on directions parallel and perpendicular to the signal wave vector, becomes

$$\Delta k_{\mathrm{par}}=k_p\cos\alpha-k_s-k_i\cos\Omega=0, \tag{31a}$$

$$\Delta k_{\mathrm{perp}}=k_p\sin\alpha-k_i\sin\Omega=0. \tag{31b}$$

Note that the angle Ω is not fixed, but depends on the signal wavelength. If the signal frequency increases by $\Delta\omega$, the

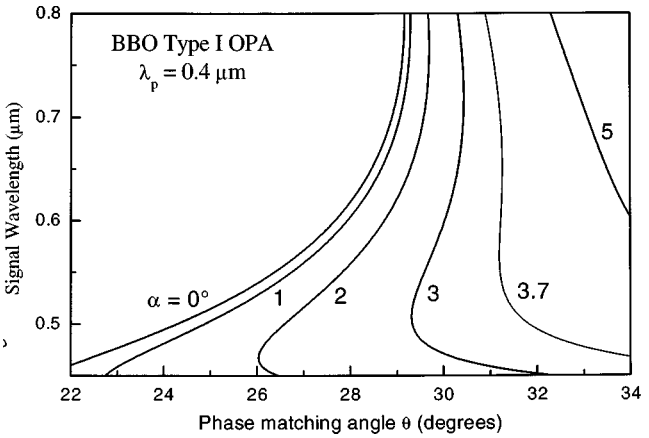

FIG. 17. Phase-matching curves for a noncollinear type I BBO OPA pumped at 0.4 μm, as a function of the pump-signal angle α.

idler frequency decreases by $\Delta\omega$ and the wave vector mismatches along the two directions can be approximated, to the first order, as

$$\Delta k_{\mathrm{par}} \cong -\frac{\partial k_s}{\partial \omega_s}\Delta\omega + \frac{\partial k_i}{\partial \omega_i}\cos\Omega\,\Delta\omega - k_i \sin\Omega\,\frac{\partial \Omega}{\partial \omega_i}\Delta\omega, \tag{32a}$$

$$\Delta k_{\mathrm{perp}} \cong \frac{\partial k_i}{\partial \omega_i}\sin\Omega\,\Delta\omega + k_i\cos\Omega\,\frac{\partial \Omega}{\partial \omega_i}\Delta\omega. \tag{32b}$$

To achieve broadband phase matching, both Δk_{par} and Δk_{perp} must vanish. Upon multiplying Eq. (32a) by $\cos\Omega$ and Eq. (32b) by $\sin\Omega$ and adding the results, we get

$$\frac{\partial k_i}{\partial \omega_i} - \cos\Omega\,\frac{\partial k_s}{\partial \omega_s} = 0 \tag{33}$$

which is equivalent to

$$\nu_{\mathrm{gs}} = \nu_{\mathrm{gi}}\cos\Omega. \tag{34}$$

Equation (34) shows that broadband phase matching can be achieved for a signal-idler angle Ω such that the signal group velocity equals the projection of the idler group velocity along the signal direction. This effect is shown pictorially in Fig. 16: for a collinear geometry [Fig. 16(b)], signal and idler moving with different group velocities get quickly separated giving rise to pulse lengthening and bandwidth reduction, while in the noncollinear case [Fig. 16(c)] the two pulses manage to stay effectively overlapped. Note that Eq. (34) can be satisfied only if $\nu_{\mathrm{gi}} > \nu_{\mathrm{gs}}$; this is, however, always the case in the commonly used type I phase matching in negative uniaxial crystals, where both signal and idler see the ordinary refractive index. Equation (34) allows to determine the signal-idler angle Ω required for broadband phase matching; from a practical point of view, it is more useful to know the pump-signal angle α, which is given by

$$\alpha = \mathrm{arc}\,\sin\left(\frac{1-\nu_{\mathrm{gs}}^2/\nu_{\mathrm{gi}}^2}{1+2\,\nu_{\mathrm{gs}} n_s \lambda_i/\nu_{\mathrm{gi}} n_i \lambda_s + n_s^2\lambda_i^2/n_i^2\lambda_s^2}\right)^{1/2}. \tag{35}$$

As an example, in a type I BBO OPA pumped at $\lambda_p = 0.4\ \mu$m for a signal wavelength $\lambda_s = 0.6\ \mu$m broadband phase matching is achieved for $\alpha = 3.7°$. To better illustrate the effect of noncollinear phase matching, in Fig. 17 we plot,

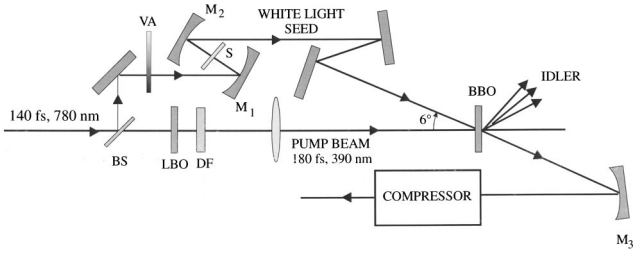

FIG. 18. Scheme of a noncollinear visible OPA. BS: beam splitter; VA: variable attenuator; *S*: 1-mm-thick sapphire plate; DF: dichroic filter; M_1, M_2, M_3, spherical mirrors.

for a type I BBO OPA pumped at 0.4 μm, the phase matching angle θ_m as a function of signal wavelength for different values of pump-signal angle α. For a collinear configuration ($\alpha = 0°$) θ_m shows a strong dependence on the signal wavelength so that, for a fixed crystal orientation, phase matching can be achieved only over a narrow signal frequency range. By going to a noncollinear configuration and increasing α, the wavelength dependence of θ_m becomes progressively weaker until, for the optimum value $\alpha = 3.7°$, a given crystal orientation ($\theta \cong 31.3°$) allows to achieve simultaneously phase matching over an ultrabroad bandwidth, extending from 0.5 to 0.75 μm. Note that, in this configuration, the symmetry between signal and idler is lost, because they propagate at different angles.

This favorable property of the noncollinear geometry for broadband parametric amplification was first recognized by Gale *et al.*[98–101] and was exploited to build broadband OPOs generating pulses as short as 13 fs; more recently, the same concept was extended by several research groups to OPAs seeded by the white-light continuum.[102–113] A schematic of the experimental setup of an ultrabroadband noncollinear OPA (NOPA) is reported in Fig. 18.[103,106,109] The system is pumped by an amplified Ti:sapphire laser, generating 140 fs pulses at 0.78 μm and 1 kHz repetition rate with energy up to 500 μJ. The pump pulses (0.39 μm wavelength, 10 μJ energy, $\approx$180 fs duration) are obtained by frequency doubling a fraction of the light in a 1-mm-thick lithium triborate crystal. The seed pulses are generated by focusing another small fraction of the FW beam, with energy of approximately 2 μJ, into a 1-mm-thick sapphire plate; by carefully controlling the energy incident on the plate (using a variable-optical-density attenuator) and the position of the plate around the focus, a highly stable single-filament white-light continuum is generated. To avoid the introduction of additional chirp, reflective optics are employed to guide the white light to the amplification stage. Parametric gain is achieved in a 1-mm-thick BBO crystal, cut at $\theta = 32°$, using a single-pass configuration to increase the gain bandwidth. The chosen crystal length is close to the pulse-splitting length for signal and pump in the wavelength range of interest. The white light seed is imaged into the BBO crystal by spherical mirror M_2, with a spot size nearly matching that of the pump beam. The amplified pulses have energy of approximately 2 μJ, peak-to-peak fluctuations of less than 7% and maintain a good TEM_{00} beam quality. Higher energies, up to $\approx$10 μJ, can be extracted by a second pass in the BBO crystal. After the gain stage the amplified pulses are collimated by the

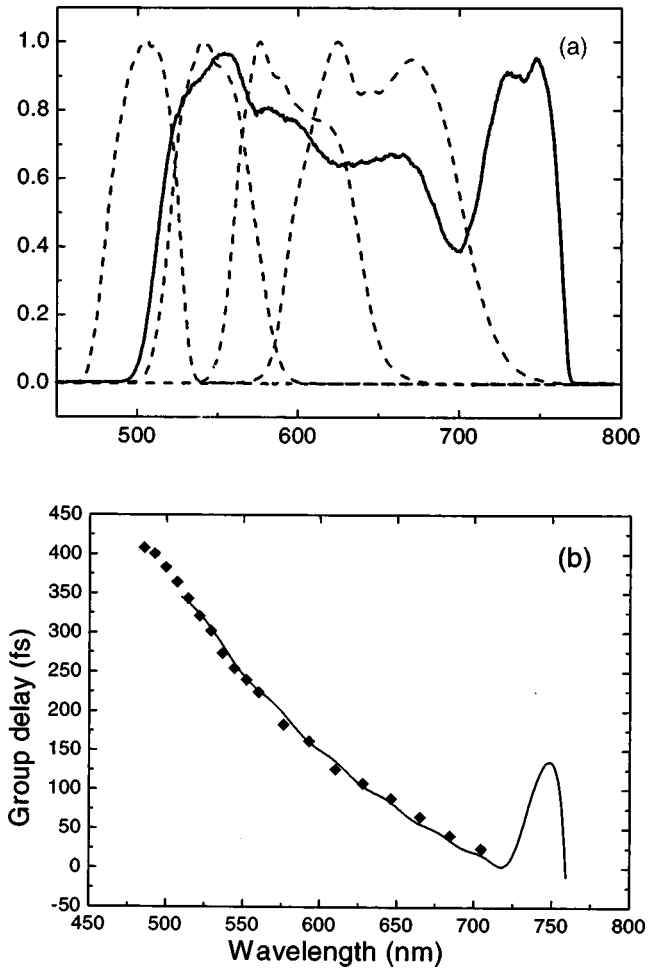

FIG. 19. (a) Solid line: NOPA spectrum under optimum alignment conditions; dashed line: sequence of spectra obtained by increasing the white light chirp; (b) points: measured GD of the NOPA pulses; dashed line: GD after ten bounces on the ultrabroadband chirped mirrors.

spherical mirror M_3 and sent to the compressor. This design is quite similar to the one reported in Sec. III B for a visible OPA, the main differences being the noncollinear geometry and the use of reflective optics to prevent pulse chirping. An accurate numerical modeling of the NOPA operation can be found in Ref. 114.

The NOPA pulse bandwidth strongly depends on the system alignment and on the chirp of the white-light seed. A typical spectrum obtained under optimum alignment conditions is shown in Fig. 19(a) as a solid line: it extends over a FWHM bandwidth of 180 THz and is virtually not tunable, since it covers the maximum available gain bandwidth. Experimentally, this condition can be easily achieved by adjusting the pump-signal angle to match the apex angle of the strong parametric superfluorescence cone[54] emitted by the BBO crystal when illuminated by the pump pulse. Narrower gain bandwidths, which may be required for some experiments, can be simply achieved by detuning the pump-seed angle from the optimum value and/or deliberately increasing the white light chirp: in this case, the NOPA can be tuned by slightly tilting the BBO crystal and/or varying the pump-seed delay. A typical sequence of amplified pulse spectra obtained under these conditions is shown in Fig. 19(a) as dashed lines.

The NOPA generates pulses with very broad bandwidths and thus potentially very short: to obtain the minimum pulse duration compatible with their bandwidth (the so-called transform-limited duration), however, their phase characteristics must be accurately controlled. The group delay (GD) versus frequency characteristics of the pulses generated by the setup of Fig. 18 is shown in Fig. 19(b). The GD the amplified pulses was measured by upconversion with a 10 nm spectral slice of the pulse, selected with an interference filter and having approximately 70 fs FWHM duration. After the upconverting crystal, an UV monochromator allowed us to determine the relative arrival times of different frequency components of the pulse. The measurement gives an overall GD of ~400 fs between the red and the blue components of the spectrum; the main contributions to the dispersion are the sapphire plate, the BBO crystal, and the path (~3.5 m) in air. Accurately correcting the phase over such broad bandwidths poses a challenge on the compression system and different approaches have been proposed. Standard Brewster-cut prism pairs can be used to compress the narrower bandwidth pulses down to a duration of 10–15 fs;[102–105] for broader bandwidths, thin prism sequences,[106] prism-grating[107] and prism-chirped mirror combinations,[108] or adaptive pulse compressors[115,116] were used. These systems show different performance in terms of corrected bandwidth and energy throughput. The shortest pulses generated by the NOPA were obtained by a prism-chirped mirror combination and have a nearly transform-limited duration of 4.4 fs.[108] Note the dramatic shortening of the pulsewidths with respect to the pump pulse duration, which is in the 100 fs range. As a matter of fact, using short pump pulses does not help in getting shorter pulses from the OPA, but on the contrary could be detrimental to the broadband amplification process, because of the reduced temporal overlap between the pump pulses and the chirped white-light seed.

A simple and experimentally convenient compressor design employs exclusively chirped dielectric mirrors,[117,118] with dispersion characteristics tailored to compensate for the NOPA GD: this approach, besides the high energy throughput and the broadband phase correction, greatly simplifies the system design, allowing for compactness, reproducibility and insensitivity to misalignment which are of great importance in practical applications.[111,113] As an example, we show in Fig. 19(b) as a solid line the opposite of the GD generated by ten bounces on chirped mirrors which were custom designed to compensate for the NOPA dispersion: it can be seen that it matches the required GD very accurately over the wavelength range 0.51–0.71 μm, with a root-mean-square deviation of only 1.8 fs.

For ultrabroadband pulses with duration in the sub-10 fs regime, traditional autocorrelation techniques, which require an *a priori* knowledge of the pulse shape, provide only rough estimates of the pulse duration. An accurate pulse characterization requires full knowledge of the amplitude and phase of the pulse, and ideally (though less commonly in practice) knowledge of the variations of the parameters across the pulse profile. Amplitude and phase can be measured in the time-frequency domain using frequency-resolved optical gating (FROG),[119] pulse spectral phase can be measured using

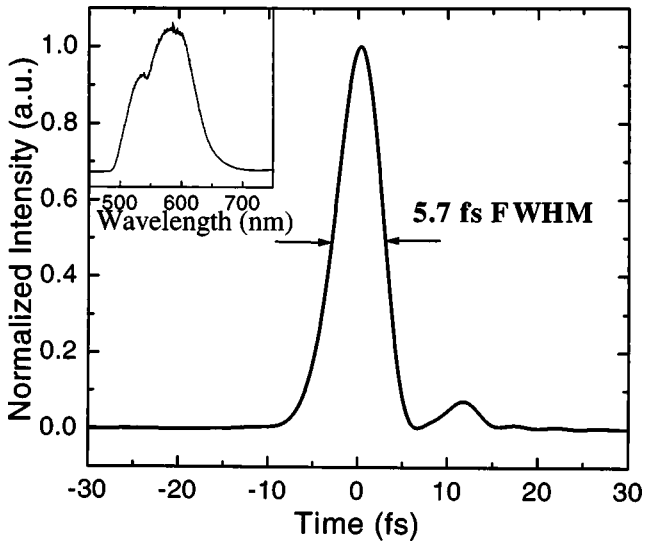

FIG. 20. Reconstructed temporal intensity of the compressed NOPA pulse measured by the SPIDER technique. The inset shows the corresponding pulse spectrum.

spectral interferometry for direct electric field reconstruction (SPIDER),[120] and combined with a separate spectral amplitude measurement from a spectrometer to obtain a time-domain reconstruction of the pulse. For the pulses generated by the NOPA shown in Fig. 18 and compressed by the chirped mirrors, a full amplitude and phase characterization was achieved using the SPIDER technique.[113] A typical reconstructed pulse amplitude profile is reported in Fig. 20, corresponding to a 5.7 fs pulse duration: its shape is remarkably clean and nearly free of side lobes, indicating the good quality of the compressor. Using the FROG technique, a pulse duration as short as 4 fs was recently measured.[116]

So far we have discussed only the signal pulses generated by the NOPA; the idler pulses have a bandwidth equal to the signal pulses and are therefore potentially very short. However, Eq. 31(b) shows that the emission angle Ω of the idler beam is wavelength dependent, so that the idler pulse presents a large angular spectral dispersion. It is, however, possible to compensate for it by use of a suitable grating-cylindrical mirror combination;[107,110] subsequent pulse compression using a standard Brewster-cut prism pair makes it possible to generate sub-10 fs pulses in the near-IR wavelength range.

B. Ultrabroadband near-infrared optical parametric amplifier

As an alternative to using the idler of the NOPA, few-optical-cycle pulses in the near-IR can be generated by OPAs pumped by the FW of a Ti:sapphire laser, using short pump pulses and exploiting nonlinear pulse compression effects. We will report on two OPA designs for short pulse generation, exploiting respectively types II and I phase matching. Both schemes generate the short pulses directly from the OPA, without using pulse compressors.

The first design, shown in Fig. 21,[121] is pumped by a standard amplified Ti:sapphire laser, which provides 140 fs, 500 μJ energy pulses at 0.78 μm at 1 kHz repetition rate.

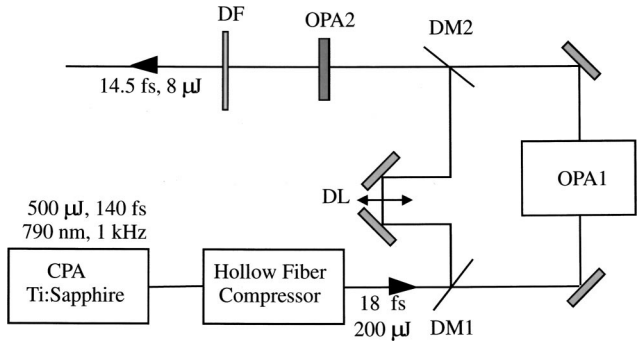

FIG. 21. Scheme of an ultrabroadband near-IR OPA. DM1, DM2: dichroic mirrors; DL: delay line; DF: dichroic filter.

The amplified pulses are coupled into a 300 μm diameter, 60 cm long, argon-filled fused-silica hollow fiber. The pulses emerging from the fiber, frequency broadened by self phase modulation, are then compressed down to 18 fs by a double pass through a Brewster-cut quartz prism pair. Pulse energy after compression is 200 μJ. Parametric light conversion is obtained in a three-pass optical parametric generation and amplification system based on two BBO crystals, cut for type II collinear phase matching ($\theta = 27°$). The seed pulse is formed by parametric superfluorescence and subsequent amplification in OPA1, designed in two-pass configuration employing a single 5 mm long type II phase-matching BBO crystal pumped by $\sim$100 μJ pulses. The power amplifier OPA2 is pumped by $\sim$100 μJ pulses, matched with seed pulses in time and space by means of a delay line and a dichroic mirror. Using a 1 mm long BBO crystal, pulses as short as 14.5 fs (see Fig. 22 for a typical pulse autocorrelation), with a broad spectrum centered at 1.5 μm, are obtained. Pulse energy is 8 μJ with peak to peak fluctuations of less than 15%. The observed pulse compression is in good agreement with that predicted by numerical simulations and is due to a nonlinear temporal reshaping induced by the interplay of GVM between the interacting pulses (signal and idler pulses are moving in opposite directions with roughly

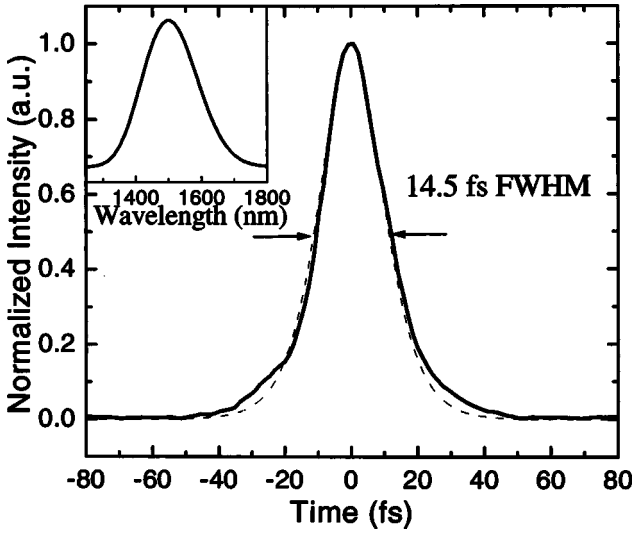

FIG. 22. Noncollinear autocorrelation of the pulses generated by the ultrabroadband near-IR OPA shown in Fig. 21. The inset shows the corresponding pulse spectrum.

the same velocity with respect to the pump pulse) and pump pulse depletion at high conversion efficiency. The extraction of higher energies or the achievement of even larger pulse compression are limited by the onset of third order nonlinear effect in the BBO crystals.

The second design is pumped by ≈40 fs pulses from an amplified Ti:sapphire laser and seeded by a white-light continuum generated in a sapphire plate.[122,123] Parametric amplification takes place in two stages using type I BBO crystals and generates pulses with energies greater than 50 μJ and duration as short a 20 fs. The shortening by a factor of 2 of the OPA pulses with respect to the pump pulses can be explained as follows: in the last OPA stage, after reaching a maximum energy the signal wave starts to recombine with the idler to generate, by backconversion, some pump radiation. Due to GVM effects (in type I phase-matching signal and idler pulses are moving in the same direction with respect to the pump) only the trailing edge of the signal recombines, giving rise to an effective saturable absorber effect which shortens the pulse.

V. CHIRPED PULSE OPTICAL PARAMETRIC AMPLIFICATION

We have seen that ultrafast OPAs have the capability to generate broadly tunable femtosecond pulses with moderate energy, which can be used for time-resolved spectroscopy and other nonlinear optics experiments. In this paragraph we describe an application of OPAs to large-scale amplification systems, which holds promise to replace the CPA scheme for the generation of the highest peak powers and intensities.

There is a great interest in the generation of ever increasing laser peak powers and focused intensities, for a number of current and potential applications. Using the CPA technique, peak powers in excess of 1 PW and intensities greater than 10^{21} W/cm^2 have been demonstrated; to scale this performance to even higher levels, a number of issues must be faced in conventional CPA systems. Since the energy levels are approaching the damage threshold of the compressor gratings, significant increases of the peak power can be only achieved by shortening the pulse duration, which in turn requires an increase of the gain bandwidth. For strongly driven amplifying media, however, the phenomenon of gain narrowing reduces the available bandwidth. In addition, prepulse due to amplified spontaneous emission spoils the temporal pulse contrast, and the large linear and nonlinear phases accumulated in the long paths through the amplifying media prevent transform-limited pulse recompression and diffraction-limited focusing. A novel high power amplification scheme, solving most of these problems, was recently proposed by Ross *et al.*, based on the seminal work by Dubietis *et al.*,[124] and termed OPCPA. In this scheme parametric gain is achieved by coupling a quasimonochromatic high energy pump field (such as, for example, a nanosecond pulse generated by a neodymium laser) to a chirped, low energy broadband seed field in a nonlinear crystal.[125–127] If the seed pulse is sufficiently stretched, good energy extraction from the pump field can be achieved, and subsequent recompression makes it possible to reach very high peak powers. The

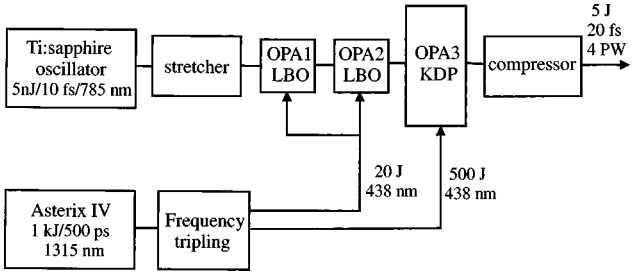

FIG. 23. Scheme of an OPCPA stage pumped by the Asterix IV iodine laser.

parametric amplification process, in the noncollinear geometry, can provide gain bandwidths well in excess of those of conventional amplifiers and could sustain pulse spectra corresponding to a transform-limited duration of ≈5 fs. High energies are possible by using large nonlinear crystals, such as potassium dihydrogen phosphate (KDP), which can be grown to sizes of tens of centimeters. These crystals should be capable of withstanding pump energies of hundreds of joules. In addition the OPCPA has the capability of providing a high gain in a relatively short path; for example, an LBO crystal pumped by 0.5 ns pulses at 0.526 μm, at intensities below the damage threshold, can have a gain coefficient of 12 cm^{-1}. This short path length allows a compact, tabletop amplifier setup and also minimizes the linear and nonlinear phase distortions and ensures an excellent temporal and spatial quality of the pulses. Finally, the very low amplified spontaneous emission level guarantees an excellent pulse contrast, and the almost complete absence of thermal loading on the crystals eliminates spatial aberration effects on the beams.

The OPCPA concept is very promising and has been already implemented in a proof-of-principle experiment to generate TW-level pulses; in a low repetition rate system pumped by a Nd:glass laser chain, 0.5 J amplified stretched pulses were obtained, subsequently recompressed to 300 fs duration.[127] More recently, using as pump a commercial *Q*-switched Nd:yttrium–aluminum–garnet laser, 31 mJ pulses with 300 fs duration were obtained using a three-pass OPCPA, using just 40 mm of gain material.[128] In the following we briefly describe the design of an OPCPA[129] pumped by the high-power iodine laser Asterix IV, a conceptual scheme of which is shown in Fig. 23. The Asterix IV pump laser delivers at the fundamental wavelength (1.315 μm) up to 1.2 kJ of energy in pulses with a duration of 500 ps; the beam can be efficiently frequency tripled to generate over 500 J of energy at 0.438 μm. The 10 fs seed pulses are generated by a Ti:sapphire oscillator and then stretched to several hundreds picoseconds; parametric amplification takes place in three stages, using a noncollinear interaction geometry, and telescopes increase the beam size after each stage. The first two stages employ LBO because of its high nonlinear coefficient and broad amplification bandwidth, while the last stage uses KDP because this nonlinear crystal can be grown in the large sizes (≈30 cm) required to keep the fluence below the damage threshold. After the compressor, energies of 100 J with pulse duration of 20 fs are expected, corresponding to a peak power of 5 PW and to a focused intensity of 10^{23} W/cm^2. In principle, these performances are

well in excess of those achievable with state of the art CPA systems; whether the OPCPA scheme will fulfill its promises still remains to be tested. Some possible problems which may arise in its practical implementation are: thermal loading due to residual absorption from the nonlinear crystals, optical damage of the crystals, high alignment sensitivity, and low pulse-to-pulse stability.

Finally, the OPCPA concept was applied successfully by Galvanauskas *et al.* to amplify the output of a femtosecond Er-doped fiber laser[130] in a very compact all-solid-state system, achieving subpicosecond microjoule-level pulses. Quasi phase matching in a periodically poled $LiNbO_3$ crystal, giving a nonlinear coefficient about an order of magnitude larger than in BBO, is exploited to achieve sufficiently high gains at pump intensities below the damage threshold.

VI. DISCUSSION

We have seen in this review article that ultrafast OPA technology has matured, making it possible to extend considerably the tuning range of femtosecond Ti:sapphire laser systems. Some OPA designs have become standard and are even commercially available. In particular, near-IR OPAs (pumped by the FW of a Ti:sapphire laser) offer tunability from 1.1 to 2.5 μm with several tens of microjoule energy, while visible OPAs (pumped by the SH of a Ti:sapphire laser) are tunable from 0.45 to 2.5 μm with somewhat lower energies. Typical pulse widths obtainable from these systems are in the 50–200 fs range, depending on the specific design and the pump pulse duration. More advanced schemes and DFG or upconversion techniques allow extending the tunability to the mid-IR range, out to 12 μm, and the UV range.

These schemes generate so called ''narrow-bandwidth'' pulses, i.e., pulses with a bandwidth which is a small fraction of the optical carrier frequency, that are tunable over a broad frequency range. However, if the proper phase matching conditions are achieved, the OPG process can have a very broad bandwidth and OPAs can generate pulses with a bandwidth which is comparable to the carrier frequency: if properly compressed, these pulses contain only a few carrier cycles under their envelope and have duration well below 10 fs. Ultrabroadband OPAs, also thanks to their reliability and simplicity of operation, are becoming established tools for ultrafast spectroscopy with extreme temporal resolution.[131–133] The gain in temporal resolution comes at the expense of a loss in spectral selectivity and also in frequency tunability, if the OPG bandwidth is fully exploited.

OPAs also have the capability of providing very high gains over ultrabroad bandwidths: this characteristics, together with the relatively short material path, negligible thermal loading of the crystals, low linear and nonlinear phase distortions, and low levels of amplified spontaneous emission, make them very attractive candidates for large-scale, high peak power amplifiers. The OPCPA concept has not yet been demonstrated experimentally, but it holds promise to increase the peak powers available from lasers well above the current limit of 1 PW.

OPAs can find also an interesting application in the field of high capacity optical communication systems. Wavelength division multiplexing systems find their main limitation in the bandwidth of Er-doped fiber amplifiers, which is currently only 50–80 nm around the wavelength of 1.55 μm, and cannot cover the full transmission window of low-loss silica fibers (1.2–1.7 μm). OPAs can in principle extend this bandwidth. However, in order to operate at the low peak power levels typical of optical communications systems, very high nonlinearities are required. This can be achieved using periodically poled $LiNbO_3$ waveguides:[134] guided propagation allows to maintain high intensities over long interaction lengths, of the order of a few centimeters, while quasi phase matching makes it possible to select the propagation direction in $LiNbO_3$ which displays the highest nonlinearity. Using these systems, parametric gains of up to 65 dB can be achieved with pump *peak* powers of only 10 W, making these devices very attractive for optical communication systems.[135]

[1] For a overview of the state of the art of ultrafast spectroscopy, see for example: *Ultrafast Phenomena XII*, Springer Verlag Series in Chemical Physics Vol. 66, edited by T. Elsaesser, S. Mukamel, M. M. Murnane, and N. F. Scherer (Springer, Berlin, 2001).
[2] T. Brabec and F. Krausz, Rev. Mod. Phys. **72**, 545 (2000).
[3] J. P. Zhou, G. Taft, C. P. Huang, M. M. Murnane, H. C. Kapteyn, and I. P. Christov, Opt. Lett. **19**, 1149 (1994).
[4] A. Stingl, M. Lenzner, C. Spielmann, F. Krausz, and R. Szipocs, Opt. Lett. **20**, 602 (1995).
[5] G. Steinmeyer, D. H. Sutter, L. Gallmann, N. Matuschek, and U. Keller, Science **286**, 1507 (1999).
[6] R. L. Fork, B. I. Greene, and C. V. Shank, Appl. Phys. Lett. **38**, 671 (1981).
[7] D. E. Spence, P. N. Kean, and W. Sibbett, Opt. Lett. **16**, 42 (1991).
[8] D. Strickland and G. Mourou, Opt. Commun. **56**, 219 (1985).
[9] S. Backus, C. Durfee, M. M. Murnane, and H. C. Kapteyn, Rev. Sci. Instrum. **69**, 1207 (1998).
[10] D. Eimerl, L. Davis, S. Velsko, E. K. Graham, and A. Zalkin, J. Appl. Phys. **62**, 1968 (1987).
[11] C. Chen, Y. Wu, A. Jiang, B. Wu, G. You, R. Li, and S. Lin, J. Opt. Soc. Am. B **6**, 616 (1989).
[12] S. Lin, Z. Sun, B. Wu, and C. Chen, J. Appl. Phys. **67**, 634 (1990).
[13] J. Y. Zhang, J. Y. Huang, Y. R. Shen, and C. Chen, J. Opt. Soc. Am. B **10**, 1758 (1993).
[14] A. Borsutzky, R. Brünger, Ch. Huang, and R. Wallenstein, Appl. Phys. B: Photophys. Laser Chem. **52**, 55 (1991).
[15] J. A. Giordamaine and R. C. Miller, Phys. Rev. Lett. **14**, 973 (1965).
[16] R. L. Byer and R. L. Herbst, in *Nonlinear Infrared Generation*, edited by Y. R. Shen (Springer, Berlin, 1977), p. 96.
[17] R. A. Baumgartner and R. L. Byer, IEEE J. Quantum Electron. **15**, 432 (1979).
[18] Y. R. Shen, *The Principles of Nonlinear Optics* (Wiley, New York, 1984).
[19] R. Boyd, *Nonlinear Optics* (Academic, New York, 1992).
[20] In the OPG process, signal and idler beams play an interchangeable role. Throughout this article we assume that the signal is at higher frequency, i.e., $\omega_s > \omega_i$.
[21] E. S. Wachman, D. C. Edelstein, and C. L. Tang, Opt. Lett. **15**, 136 (1990).
[22] Q. Fu, G. Mak, and H. M. van Driel, Opt. Lett. **17**, 1006 (1992).
[23] W. S. Pelouch, P. E. Powers, and C. L. Tang, Opt. Lett. **17**, 1070 (1992).
[24] P. E. Powers, R. J. Ellingson, W. S. Pelouch, and C. L. Tang, J. Opt. Soc. Am. B **10**, 2162 (1993).
[25] V. G. Dmitriev, G. G. Gurzadyan, and D. N. Nikogosyan, *Handbook of Nonlinear Optical Crystals* (Springer, Berlin, 1991).
[26] W. Koechner, *Solid-State Laser Engineering*, 4th ed. (Springer, Berlin, 1996).
[27] A. G. Akmanov, S. A. Akhmanov, R. V. Khoklov, A. I. Kovrigin, A. S. Piskarkas, and A. P. Sukhorukow, IEEE J. Quantum Electron. **QE–4**, 828 (1968).
[28] S. A. Akhmanov, V. A. Vysloukh, and A. S. Chirkin, *Optics of Femtosecond Laser Pulses* (American Institute of Physics, New York, 1992).

[29] T. B. Norris, Opt. Lett. **17**, 1009 (1992).
[30] S. E. Harris, M. K. Oshman, and R. L. Byer, Phys. Rev. Lett. **18**, 732 (1967).
[31] *The Supercontinuum Laser Source*, edited by R. R. Alfano (Springer, New York, 1989).
[32] R. L. Fork, C. V. Shank, C. Hirlimann, R. Yen, and W. J. Tomlinson, Opt. Lett. **8**, 1 (1983).
[33] A. L. Gaeta, Phys. Rev. Lett. **84**, 3582 (2000).
[34] W. Joosen, H. J. Bakker, L. D. Noordam, H. G. Muller, and H. B. van Linden van der Heuvell, J. Opt. Soc. Am. B **8**, 2537 (1991).
[35] W. Joosen, P. Agostini, G. Petite, J. P. Chambaret, and A. Antonetti, Opt. Lett. **17**, 133 (1992).
[36] G. P. Banfi, P. Di Trapani, R. Danielius, A. Piskarkas, R. Righini, and I. Sa'nta, Opt. Lett. **18**, 1547 (1993).
[37] G. P. Banfi, P. Di Trapani, R. Danielius, A. Piskarkas, R. Righini, and I. Sa'nta, Opt. Lett. **18**, 1547 (1993).
[38] G. P. Banfi, R. Danielius, A. Piskarkas, P. Di Trapani, P. Foggi, and R. Righini, Opt. Lett. **18**, 1633 (1993).
[39] R. Danielius, A. Piskarskas, A. Stabinis, G. P. Banfi, P. Di Trapani, and R. Righini, J. Opt. Soc. Am. B **10**, 2222 (1993).
[40] V. Petrov, F. Seifert, and F. Noack, Appl. Phys. Lett. **65**, 268 (1994).
[41] F. Seifert, V. Petrov, and F. Noack, Opt. Lett. **19**, 837 (1994).
[42] M. Nisoli, S. De Silvestri, V. Magni, O. Svelto, R. Danielius, A. Piskarkas, G. Valiulis, and A. Varavinicius, Opt. Lett. **19**, 1973 (1994).
[43] V. V. Yakovlev, B. Kohler, and K. R. Wilson, Opt. Lett. **19**, 2000 (1994).
[44] K. R. Wilson and V. V. Yakovlev, J. Opt. Soc. Am. B **14**, 444 (1997).
[45] J. Piel, M. Beutter, and E. Riedle, Opt. Lett. **25**, 180 (2000).
[46] R. Danielius, A. Piskarskas, P. Di Trapani, A. Andreoni, C. Solcia, and P. Foggi, Appl. Opt. **35**, 5336 (1996).
[47] V. Petrov, F. Seifert, and F. Noack, Appl. Opt. **33**, 6988 (1994).
[48] V. Petrov and F. Noack, Opt. Lett. **20**, 2171 (1995).
[49] M. K. Reed, M. K. Steiner-Shepard, and D. K. Negus, Opt. Lett. **19**, 1855 (1994).
[50] M. K. Reed, M. S. Armas, M. K. Steiner-Shepard, and D. K. Negus, Opt. Lett. **20**, 605 (1995).
[51] M. K. Reed, M. K. Steiner-Shepard, M. S. Armas, and D. K. Negus, J. Opt. Soc. Am. B **12**, 2229 (1995).
[52] S. R. Greenfield and M. R. Wasielewski, Opt. Lett. **20**, 1394 (1995).
[53] S. R. Greenfield and M. R. Wasielewski, Appl. Opt. **34**, 2688 (1995).
[54] R. Danielius, A. Piskarkas, P. Di Trapani, A. Andreoni, C. Solcia, and P. Foggi, Opt. Lett. **21**, 973 (1996).
[55] P. Di Trapani, A. Andreoni, P. Foggi, C. Solcia, R. Danielius, and A. Piskarkas, Opt. Commun. **119**, 327 (1995).
[56] P. Di Trapani, A. Andreoni, C. Solcia, G. P. Banfi, R. Danielius, A. Piskarskas, and P. Foggi, J. Opt. Soc. Am. B **14**, 1245 (1997).
[57] P. Di Trapani, A. Andreoni, C. Solcia, P. Foggi, R. Danielius, A. Dubietis, and A. Piskarkas, J. Opt. Soc. Am. B **12**, 2237 (1995).
[58] P. Matousek, A. W. Parker, P. F. Taday, W. T. Toner, and M. Towrie, Opt. Commun. **127**, 307 (1996).
[59] T. S. Sosnowski, P. B. Stephens, and T. B. Norris, Opt. Lett. **21**, 140 (1996).
[60] K. S. Wong, Z. R. Qui, H. Wang, and G. K. L. Wong, Opt. Lett. **22**, 898 (1997).
[61] V. Krylov, A. Kalintsev, A. Rebane, D. Erni, and U. P. Wild, Opt. Lett. **20**, 151 (1995).
[62] V. Krylov, O. Ollikainen, J. Gallus, U. P. Wild, A. Rebane, and A. Kalintsev, Opt. Lett. **23**, 100 (1998).
[63] V. Petrov, F. Noack, and R. Stolzenberger, Appl. Opt. **36**, 1164 (1997).
[64] F. Rotermund, V. Petrov, F. Noack, V. Pasiskevicius, J. Hellstroem, and F. Laurell, Opt. Lett. **24**, 1874 (1999).
[65] V. Petrov and F. Noack, Opt. Lett. **21**, 1576 (1996).
[66] F. Rotermund, V. Petrov, F. Noack, M. Wittmann, and G. Korn, J. Opt. Soc. Am. B **16**, 1539 (1999).
[67] V. Petrov, F. Rotemund, and F. Noack, Appl. Opt. **37**, 8504 (1998).
[68] V. Petrov, F. Rotermund, F. Noack, and P. Schunemann, Opt. Lett. **24**, 414 (1999).
[69] F. Rotermund and V. Petrov, Opt. Lett. **25**, 746 (2000).
[70] F. Seifert, V. Petrov, and M. Woerner, Opt. Lett. **19**, 2009 (1994).
[71] M. K. Reed and M. K. Steiner Shepard, IEEE J. Quantum Electron. **32**, 1273 (1996).
[72] B. Golubovic and M. K. Reed, Opt. Lett. **23**, 1760 (1998).
[73] M. R. X. de Barrios, R. S. Miranda, T. M. Jedju, and P. C. Becker, Opt. Lett. **20**, 480 (1995).
[74] Ch. Fattinger and D. Grischkowsky, Appl. Phys. Lett. **54**, 490 (1989).
[75] L. Xu, X.-C. Zhang, and D. H. Auston, Appl. Phys. Lett. **61**, 1784 (1992).
[76] Y. H. Lin and X. C. Zhang, J. Nonlinear Opt. Phys. Mater. **4**, 459 (1995).
[77] P. Y. Han and X.-C. Zhang, Appl. Phys. Lett. **73**, 3049 (1998).
[78] A. Bonvalet, M. Joffre, J.-L. Martin, and A. Migus, Appl. Phys. Lett. **67**, 2907 (1995).
[79] M. Joffre, A. Bonvalet, A. Migus, and J.-L. Martin, Opt. Lett. **21**, 964 (1996).
[80] R. A. Kaindl, D. C. Smith, M. Joschko, M. P. Hasselbeck, M. Woerner, and T. Elsaesser, Opt. Lett. **23**, 861 (1998).
[81] R. A. Kaindl, F. Eickemeyer, M. Woerner, and T. Elsaesser, Appl. Phys. Lett. **75**, 1060 (1999).
[82] J.-P. Likforman, M. Mehendale, D. M. Villeneuve, M. Joffre, and P. B. Corkum, Opt. Lett. **26**, 99 (2001).
[83] L. D. Ziegler, J. Morais, Y. Zhou, S. Constantine, M. K. Reed, M. K. Steiner-Shepard, and D. Lommel, IEEE J. Quantum Electron. **34**, 1758 (1998).
[84] A. Kummorw, M. Wittmann, F. Tschirschwitz, G. Korn, and E. T. J. Nibbering, Appl. Phys. B: Lasers Opt. **71**, 885 (2000).
[85] G. C. Bhar, P. Kumbhakar, U. Chatterjee, A. M. Rudra, and A. Nagahori, Opt. Commun. **176**, 199 (2000).
[86] C. G. Durfee III, S. Backus, M. M. Murnane, and H. C. Kapteyn, Opt. Lett. **22**, 1565 (1997).
[87] C. G. Durfee III, S. Backus, H. C. Kapteyn, and M. M. Murnane, Opt. Lett. **24**, 697 (1997).
[88] C. G. Durfee, A. Rundquist, S. Backus, Z. Chang, C. Herne, H. C. Kapteyn, and M. M. Murnane, J. Nonlinear Opt. Phys. Mater. **8**, 211 (1999).
[89] L. Misoguti, S. Backus, C. G. Durfee, R. Bartels, M. M. Murnane, and H. C. Kapteyn, Phys. Rev. Lett. **87**, 013601 (2001).
[90] S. Meyer, B. N. Chichkov, and B. Wellegehausen, J. Opt. Soc. Am. B **16**, 1587 (1999).
[91] C. Reinhardt, B. N. Chichkov, and B. Wellegehausen, Opt. Lett. **25**, 1043 (2000).
[92] S. Meyer, B. N. Chichkov, B. Wellegehausen, and A. Sanpera, Phys. Rev. A **61**, 063811 (2000).
[93] S. Meyer, H. Eichmann, T. Menzel, S. Nolte, B. Wellegehausen, B. N. Chichkov, and C. Momma, Phys. Rev. Lett. **76**, 3336 (1996).
[94] A. L'Huillier and P. Balcou, Phys. Rev. Lett. **70**, 774 (1993).
[95] J. J. Macklin, J. D. Kmetec, and C. L. Gordon III, Phys. Rev. Lett. **70**, 766 (1993).
[96] H. Eichmann, S. Meyer, K. Riepl, C. Momma, and B. Wellegehausen, Phys. Rev. A **50**, R2834 (1994).
[97] M. B. Gaarde, P. Antoine, A. Persson, B. Carrè, A. L'Huillier, and C. G. Wahlström, J. Phys. B **29**, L163 (1996).
[98] T. J. Driscoll, G. M. Gale, and F. Hache, Opt. Commun. **110**, 638 (1994).
[99] G. M. Gale, M. Cavallari, T. J. Driscoll, and F. Hache, Opt. Lett. **20**, 1562 (1995).
[100] G. M. Gale, M. Cavallari, and F. Hache, J. Opt. Soc. Am. B **15**, 702 (1998).
[101] G. M. Gale, M. Cavallari, and F. Hache, IEEE J. Sel. Top. Quantum Electron. **4**, 224 (1998).
[102] T. Wilhelm, J. Piel, and E. Riedle, Opt. Lett. **22**, 1494 (1997).
[103] G. Cerullo, M. Nisoli, and S. De Silvestri, Appl. Phys. Lett. **71**, 3616 (1997).
[104] A. Shirakawa and T. Kobayashi, Appl. Phys. Lett. **72**, 147 (1998).
[105] A. Shirakawa and T. Kobayashi, IEICE Trans. Electron. **E81-C**, 246 (1998).
[106] G. Cerullo, M. Nisoli, S. Stagira, and S. De Silvestri, Opt. Lett. **23**, 1283 (1998).
[107] A. Shirakawa, I. Sakane, and T. Kobayashi, Opt. Lett. **23**, 1292 (1998).
[108] A. Shirakawa, I. Sakane, M. Takasaka, and T. Kobayashi, Appl. Phys. Lett. **74**, 2268 (1999).
[109] G. Cerullo, M. Nisoli, S. Stagira, S. De Silvestri, G. Tempea, F. Krausz, and K. Ferencz, Opt. Lett. **24**, 1529 (1999).
[110] T. Kobayashi and A. Shirakawa, Appl. Phys. B: Lasers Opt. **70**, S239 (2000).
[111] G. Cerullo, M. Nisoli, S. Stagira, S. De Silvestri, G. Tempea, F. Krausz, and K. Ferencz, Appl. Phys. B: Lasers Opt. **70**, S253 (2000).
[112] E. Riedle, M. Beutter, S. Lochbrunner, J. Piel, S. Schenkl, S. Spörlein, and W. Zinth, Appl. Phys. B: Lasers Opt. **B71**, 457 (2000).
[113] M. Zavelani-Rossi *et al.*, Opt. Lett. **26**, 1155 (2001).
[114] S. Reisner and M. Gutman, J. Opt. Soc. Am. B **16**, 1801 (1999).
[115] D. Zeidler, T. Hornung, D. Proch, and M. Motzkus, Appl. Phys. B: Lasers Opt. **70**, S125 (2000).

[116] A. Baltuska, T. Fuji, and T. Kobayashi, Opt. Lett. **27**, 306 (2002).
[117] R. Szipöcs, K. Ferencz, C. Spielmann, and F. Krausz, Opt. Lett. **19**, 201 (1994).
[118] F. X. Kärtner *et al.*, Opt. Lett. **22**, 831 (1997).
[119] R. Trebino, K. W. DeLong, D. N. Fittinghoff, J. N. Sweetser, M. A. Krumbügel, B. A. Richman, and D. J. Kane, Rev. Sci. Instrum. **68**, 3277 (1997).
[120] C. Iaconis and I. A. Walmsley, Opt. Lett. **23**, 792 (1998).
[121] M. Nisoli, S. Stagira, S. De Silvestri, O. Svelto, G. Valiulis, and A. Varavinicius, Opt. Lett. **23**, 630 (1998).
[122] S. Fournier, R. Lopez-Martens, C. Le Blanc, E. Baubeau, and F. Salin, Opt. Lett. **23**, 627 (1998).
[123] R. Lòpez-Martens, S. Fournier, C. Le Blanc, E. Baubeau, and F. Salin, IEEE J. Sel. Top. Quantum Electron. **4**, 230 (1998).
[124] A. Dubietis, G. Jonusasuskas, and A. Piskarkas, Opt. Commun. **88**, 437 (1992).
[125] I. N. Ross, P. Matousek, M. Towrie, A. J. Langley, and J. L. Collier, Opt. Commun. **144**, 125 (1997).
[126] J. Collier, C. Hernandez-Gomez, I. N. Ross, P. Matousek, C. N. Danson, and J. Walczak, Appl. Opt. **38**, 7486 (1999).
[127] I. N. Ross *et al.*, Appl. Opt. **39**, 2422 (2000).
[128] I. Jovanovic, B. J. Comaskey, C. A. Ebbers, R. A. Bonner, and D. M. Pennington, Conference on Lasers and Electro-Optics 2001, Technical Digest, 2001, p. CPD8-C1-2.
[129] P. Matousek, B. Rus, and I. N. Ross, IEEE J. Quantum Electron. **36**, 158 (2000).
[130] A. Galvanauskas, A. Hariharan, D. Harter, M. A. Arbore, and M. M. Fejer, Opt. Lett. **23**, 210 (1998).
[131] G. Cerullo, G. Lanzani, M. Muccini, C. Taliani, and S. De Silvestri, Phys. Rev. Lett. **83**, 231 (1999).
[132] A. Sugita, T. Saito, H. Kano, M. Yamashita, and T. Kobayashi, Phys. Rev. Lett. **86**, 2158 (2001).
[133] G. Lanzani, G. Cerullo, M. Zavelani-Rossi, S. De Silvestri, D. Comoretto, G. Musso, and G. Dellepiane, Phys. Rev. Lett. **87**, 187402 (2001).
[134] M. L. Bortz, M. A. Arbore, and M. M. Fejer, Opt. Lett. **20**, 49 (1995).
[135] A. Galvanauskas, K. K. Wong, K. El Hadi, M. Hofer, M. E. Fermann, D. Harter, M. H. Chou, and M. M. Fejer, Electron. Lett. **35**, 731 (1999).